The Astrophysical Journal, 717:708–723, 2010 July 10 doi:10.1088/0004-637X/717/2/708

FEEDBACK FROM CENTRAL BLACK HOLES IN ELLIPTICAL GALAXIES. III. MODELS WITH BOTH RADIATIVE AND MECHANICAL FEEDBACK

Luca Ciotti[1], Jeremiah P. Ostriker[2,3], and Daniel Proga[4]
[1] Department of Astronomy, University of Bologna, via Ranzani 1, I-40127 Bologna, Italy
[2] Princeton University Observatory, Princeton, NJ, USA
[3] IoA, Cambridge, UK
[4] Department of Physics and Astronomy, University of Nevada, Las Vegas, NV, USA
Received 2010 March 1; accepted 2010 May 12; published 2010 June 17

ABSTRACT

We find, from high-resolution hydro simulations, that winds from active galactic nuclei effectively heat the inner parts (≈100 pc) of elliptical galaxies, reducing infall to the central black hole; and radiative (photoionization and X-ray) heating reduces cooling flows at the kpc scale. Including both types of feedback with (peak) efficiencies of $3 \times 10^{-4} \lesssim \epsilon_{\rm w} \lesssim 10^{-3}$ and of $\epsilon_{\rm EM} \simeq 10^{-1.3}$ respectively, produces systems having duty cycles, central black hole masses, X-ray luminosities, optical light profiles, and E+A spectra in accord with the broad suite of modern observations of massive elliptical systems. Our main conclusion is that mechanical feedback (including energy, momentum, and mass) is necessary but the efficiency, based on several independent arguments, must be a factor of 10 lower than is commonly assumed. Bursts are frequent at $z > 1$ and decline in frequency toward the present epoch as energy and metal-rich gas are expelled from the galaxies into the surrounding medium. For a representative galaxy of final stellar mass $\simeq 3 \times 10^{11}\, M_\odot$, roughly $3 \times 10^{10}\, M_\odot$ of recycled gas has been added to the interstellar medium (ISM) since $z \simeq 2$ and, of that, roughly 63% has been expelled from the galaxy, 19% has been converted into new metal-rich stars in the central few hundred parsecs, and 2% has been added to the central supermassive black hole (SMBH), with the remaining 16% in the form of hot X-ray emitting ISM. The bursts occupy a total time of ≃170 Myr, which is roughly 1.4% of the available time. Of this time, the central supermassive black hole would be seen as a UV or optical source for ≃45% and ≃71% of the time, respectively. Restricting to the last 8.5 Gyr, the bursts occupy ≃44 Myr, corresponding to a fiducial duty cycle of $\simeq 5 \times 10^{-3}$.

Key words: accretion, accretion disks – black hole physics – galaxies: active – galaxies: nuclei – galaxies: starburst – quasars: general

Online-only material: color figures

1. INTRODUCTION

In a previous paper (Ciotti et al. 2009b, hereafter Paper I), we described in detail the physical processes that are included in our current hydrodynamical modeling of the co-evolution of a massive elliptical galaxy that contains a central supermassive black hole (hereafter SMBH). Important elements include gas shed by evolving stars, cooling-flow-driven infall to the central regions of this gas and the associated star bursts, accompanied by accretion onto the central SMBH and followed by nuclear and galactic winds driven from the galaxy. Feedback in both radiative and mechanical forms is taken into account, with the sources being the central SMBH, Type II supernova (SNII), and UV from the newly formed stars, Type Ia supernova (SNIa) from older populations, and thermalization of stellar mass losses.

To our surprise in Paper I and in the companion Paper II (Shin et al. 2010a) we found that despite the richness of the modeling we could not adequately represent the co-evolution of elliptical galaxies and their central SMBHs, using the conventional physics and *either* purely radiative or purely mechanical feedback from the central SMBHs. In retrospect, this is not surprising because both processes operate in nature, so that presumably both are required to produce outcomes in agreement with observations.

We can summarize the main results of our previous work as follows.

1. SNIa are energetically quite important and will drive winds from elliptical galaxies (e.g., Ciotti et al. 1991; Ciotti & Ostriker 2007, hereafter CO07) but are only effective on the kpc scale, where the gas densities are low. They cannot prevent cooling flows and massive accumulations of gas into the inner regions of medium to massive ellipticals when their present-day rate is in accordance with the most recent observational estimates and the time evolution follows the current theoretical indications (e.g., see Pellegrini & Ciotti 1998).
2. Radiative feedback from central SMBHs (primarily the X-ray component) and the young star generated feedback consequent to central star bursts (e.g., Thompson et al. 2005) can balance and consume the cooling-flow gas at the 10^2–10^3 pc scale, but they will not sufficiently limit the growth of the central SMBHs. These processes—radiation feedback and energy input from stellar evolution—regulate the starburst phenomenon (Ciotti & Ostriker 2001, CO07).
3. Mechanical feedback from the central SMBH on the 10^1–10^2 pc scale, mediated by a nuclear jet and the broad-line region winds (e.g., Binney & Tabor 1995; Begelman & Nath 2005; Begelman & Ruszkowski 2005; Di Matteo et al. 2005), is efficient in limiting the growth of the SMBH, but, absent the processes noted in Point 2 above, would leave elliptical galaxies with more central star formation (fed either by cooling flows or mergers) than is observed (Papers I and II).

Thus, we concluded that all three sets of processes 1, 2, and 3 acting on three different radial scales are in fact required (and, of course, as noted all three—SNIa, active galactic

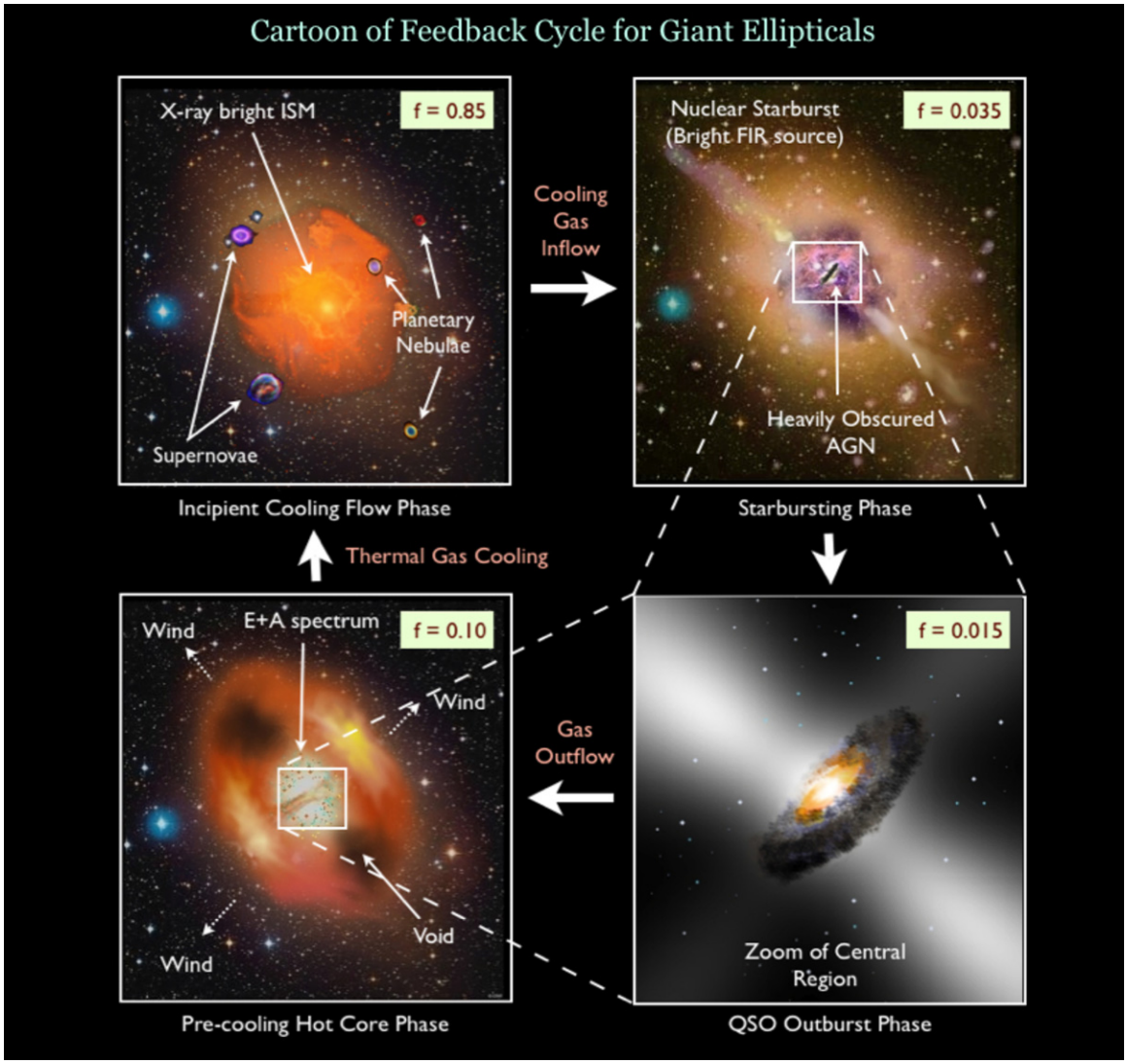

Figure 1. Four main phases of the feedback cycle in the life of a galaxy. Secondary gas from stellar evolution leads to a cooling-flow thermal instability that feeds a central SMBH, the outbursts from which lead to an expanding hot bubble which terminates the inflow. The cycle may be repeated several times, and in each box we give the characteristic duty-cycle $f_{\rm duty}$ associated with each phase in a standard simulation.

(A color version of this figure is available in the online journal.)

nuclei (AGNs) radiation, broad-line region winds—are observed phenomena) to match what we know of the properties of elliptical galaxies. Note that characteristic time scales, relevant from the observational point of view, are associated in a natural way to the different processes mentioned above. In practice, while SNIa, stellar mass losses and gas cooling in the central regions of the galaxy drive the global evolution of the galaxy gas mass budget on temporal scales of several Gyr (determined by the stellar evolution clock), AGN feedback acts on shorter time scales, as each major feedback event usually spans 10^7–10^8 yr. The simulations also revealed that each major central outburst actually consists of several feedback events, on time scales of ≈1 Myr or less, i.e., the sound crossing time of the central kpc scale region of the galaxy. Finally, the last characteristic time scale (≈0.5–1 Gyr) is that of dissipation of feedback effects on galactic scales, set by the sound crossing time over the galaxy body.

The purpose of this paper is to refine those conclusions, to show which *combined models* (i.e., in which both radiative and mechanical feedback effects are allowed) best fit observations, and finally to propose observational tests of the overall picture. We recall that all the presented simulations represent the evolution of an intermediate luminosity, isolated elliptical galaxy (i.e., no external pressure is imposed at the numerical grid outer boundary), while the case of a galaxy in a cluster will be the focus of future works. We assume, following long standing observational data and recent simulations, that the elliptical galaxy in question was made earlier and is close to its current state when the calculation begins at $z \simeq 2$ (e.g., Renzini 2006; Naab et al. 2007).

The overall situation is inherently complex, and so, before diving into the details of our new computations, it may be useful to present a very rough, cartoon-level picture of the results. In Figure 1, the arrows show the direction of time as the galaxy/SMBH passes through four (of the many) phases of evolution, and, since we are describing a cyclic phenomenon, we can start at any point. A very rough estimate of the fraction of a cycle spent in any given phase is shown in the sub-boxes at the upper right of each box as a "duty cycle," $f_{\rm duty}$.

1. We arbitrarily begin at the upper left-hand corner of the figure in the more or less quiescent phase that occupies most of the time for normal elliptical galaxies. Planetary nebulae

and other sources of secondary gas, processed through stellar evolution, are added to the ambient gas everywhere in the galaxy at a rate proportional to the stellar density and with an energy due to the stellar motions which guarantees that, when the gas is thermalized, it will be approximately at the local "virial" temperature without need for extra energy input or output. Supernovae (SNe), primarily of type Ia are also distributed like the stars and will tend to drive a mild wind from the outer parts of the galaxy, with the inner parts being quite luminous in thermal X-rays. This is a "normal" giant elliptical galaxy.

2. But, the gas in the dense inner part of the galaxy is radiating far more energy than can be replaced by SNIa, stellar outbursts, cosmic rays, conduction or any other energy source and thus a "cooling catastrophe" occurs with a collapsing cold shell forming at ≈1 kpc from the center. As this falls toward the center, a starburst occurs of the type described by Thompson et al. (2005), and the galaxy is seen as a ultraluminous infrared galaxy (ULIRG). A radio jet may be emitted, but the AGN flareup is at first heavily obscured and the central source will only be seen in hard X-rays.
3. Gradually, the gas is consumed, as it is transformed into new stars, and some of it is driven out in a strong wind by the combined effects of feedback from the starburst and the central SMBH, which is now exposed as an optical and then UV "quasar," complete with broad-line region (hereafter BLR) wind, optically thick disk of gas, and young stars.
4. As gas is used up or blown away, a hot cavity is formed at the center of the system and, since a shock has propagated through that volume, it is essentially like a giant supernova remnant and one expects there to be particle acceleration and non-thermal radiation from the central region. This phase has been studied in detail in Jiang et al. (2010). Then, gradually this hot bubble cools and collapses and one returns to the normal elliptical phase at stage 1.

One is reminded of the Shakespearean seven ages of man in "As You Like It." To paraphrase: "And one galaxy, in its time, plays many parts"—the thermal X-ray source, the starburst, the quasar, the A+E system, etc.

This paper is organized as follows. In Section 2, we briefly summarize the main properties of the models adopted for the simulations, referring to Paper I for all details of galaxy model construction and input physics. In Section 3, we present the results obtained when adopting a fixed mechanical efficiency of the nuclear radiatively driven wind. In Section 4, we describe in detail how the different problems encountered in the models with fixed mechanical efficiency are solved in the preferred class of simulations, in which the mechanical feedback depends on the instantaneous accretion luminosity; some relevant observational properties of these last types of model are also described. Finally, in Section 5, we discuss the main results obtained, observational tests, and future developments.

2. THE MODELS

A full description of the galaxy models and the input physics adopted for the simulations is given in Paper I and in the Appendix of Paper II; a comparative summary of the present and past treatments is given in Table 1 of Paper I, while here we just recall the main properties of the specific galaxy models used in the simulations.

For ease of comparison with the results of Papers I and II, we study the main properties of a representative model characterized by an initial stellar mass $M_* = 2.9 \times 10^{11}\, M_\odot$, a Fundamental Plane effective radius $R_e = 6.9$ kpc, and a central aperture velocity dispersion $\sigma_a = 260$ km s^{-1}, immersed in a dark matter halo so that the total mass density distribution is proportional to r^{-2}, with an identical amount of stellar and dark matter within the spatial half-light radius. The stellar distribution is modeled by using a Jaffe (1983) profile,[5] and all the dynamical properties needed in the simulations are given in Ciotti et al. (2009a). The initial mass of the central SMBH is assumed to follow the present-day Magorrian relation ($M_{BH} \simeq 10^{-3} M_*$; see Magorrian et al. 1998, see also Yu & Tremaine 2002), as it is believed that the bulk of the SMBH mass is assembled during the process of galaxy formation (e.g., Haiman et al. 2004; Sazonov et al. 2005), a process which is not addressed with the present simulations. The initial conditions in this study are represented by a very low density gas at the local thermalization temperature. The establishment of such a high-temperature gas phase at early cosmological times is believed to be due to a "phase transition" when, as a consequence of star formation, the gas-to-stars mass ratio was of the order of 10% and the combined effect of shocks, SN explosions, and AGN feedback became effective in heating the gas and driving galactic winds. Several theoretical arguments and much empirical evidence, such as galaxy evolutionary models and the metal content of the intracluster medium (ICM) support this scenario (e.g., Renzini et al. 1993; Ostriker & Ciotti 2005; Di Matteo et al. 2005; Springel et al. 2005; Johansson et al. 2008). For the reasons above, in the simulation presented here (as well as in all other simulations not shown), we assume that the age of the galaxy stellar component at the beginning of the simulation is 2 Gyr old, and the simulations usually span 12 Gyr, so that the cosmic time at the end of the simulations is 14 Gyr.

We set outflow boundary conditions at the galaxy outskirts (∼250 kpc), so that the simulations represent an isolated elliptical galaxy, without the confining effect of the ICM. A central cluster galaxy would have more difficulty generating winds and would suffer from bursts of cluster gas inflow. We adopted this procedure to adhere to the standard approach followed in "cooling-flow" simulations, and to better evaluate the impact of the combined feedback by comparison with the previously explored cases, while in future explorations we will address in a more consistent way the problem of the external pressure effects, of the galaxy structural and dynamical modifications due to star formation and mass redistribution over a Hubble time, the evolution of galaxies with different initial mass and central velocity dispersion, and the compatibility of the obtained galaxies with the present-day scaling laws of elliptical galaxies (Ciotti 2009a). Separately (Shin et al. 2010b) we also illustrate the variations in evolutionary paths caused by consideration of different initial mass galaxies and differing in outer boundary conditions (in particular the stripping process corresponding to different environments). We also stress that the models here discussed are just a representative sample out of several tens of runs that have been made, characterized by different choices of the input physics parameters (often outside the currently accepted ranges).

As in Paper I, the bolometric SMBH luminosity L_{BH} produced by accretion is related to the instantaneous accretion rate $\dot{M}_{BH}$

[5] We correct a typo in Paper I. Just before Equation (2) the correct expression is $R_e = 0.7447 r_*$ for the Jaffe profile. All the related numbers in the paper and in the code are correct.

(calculated according to Equations (5)–(26) of Paper I) by a luminosity-dependent electromagnetic (EM) efficiency $\epsilon_{\rm EM}$ as

$$L_{\rm BH} = \epsilon_{\rm EM}\,\dot{M}_{\rm BH}\,c^2, \quad \epsilon_{\rm EM} = \epsilon_0 \frac{A\dot{m}}{1+A\dot{m}}, \quad \dot{m} \equiv \frac{\dot{M}_{\rm BH}}{\dot{M}_{\rm Edd}}, \quad (1)$$

where $\dot{M}_{\rm Edd} = L_{\rm Edd}/(\epsilon_0 c^2)$ is the Eddington mass accretion rate. A is a free parameter so that the "ADAF-like" efficiency scales as $\epsilon_{\rm EM} \sim \epsilon_0 A\dot{m}$ for $\dot{m} \ll A^{-1}$. In our simulations we fix $A = 100$ (see, e.g., Narayan & Yi 1994; see also Ciotti & Ostriker 2001, where a very preliminary investigation of ADAF effects on radiative feedback was carried out. Note that this transition value seems to be confirmed by recent observations, as reported in Constantin et al. 2009). We finally adopt as maximum value for the EM efficiency $\epsilon_0 = 0.1$ or 0.2 (e.g., see Noble et al. 2009). We stress that in the treatment of radiation feedback we consider, in addition to radiation pressure (whose importance is well recognized, see e.g., Nayakshin & Power 2010; King 2010, and references therein), calculated by solving the transport equation for the SMBH accretion luminosity and the starburst luminosity (CO07 and Paper I), also heating/cooling (i.e., energy) feedback (Sazonov et al. 2004, 2005).

We now briefly mention the main aspects of the mechanical feedback treatment that in the present *combined* models is added to radiative feedback. In Paper I, we introduced a nuclear wind (with fixed opening angle in Type A models and with luminosity-dependent opening angle in Type B models), and a jet (with very small and fixed opening angle), but the jet contribution was not included in the models considered in Papers I and II. Here we still neglect the jet effects on the grounds that a thin relativistic jet will largely drill through the central gas, depositing its energy at much larger radii, and non-negligible effects are expected to be relevant only in the low-luminosity, hot accretion phases characterizing late-time evolution, perhaps by further reducing the nuclear luminosity. However, as an additional piece of input physics we now present some models in which the explicit time-dependent term in the differential equation describing the mechanical feedback (Paper I, Equation (29)) is taken into account.

The common treatment of mechanical feedback (e.g., Di Matteo et al. 2005; Johansson et al. 2008) is to estimate the mass inflowing to the SMBH, multiply this by a coefficient $\epsilon_{\rm w}$ representing the efficiency of conversion of mass to (kinetic) energy following the prescription[6]

$$L_{\rm dw} = \epsilon_{\rm w}\dot{M}_{\rm BH}c^2, \quad (2)$$

and add that energy into the lower layers of the hydrodynamic simulation in thermal form. Of course, in reality there is also radial momentum added to the same zone via the outflowing wind that carries the energy to the receiving layers. A recent paper (DeBuhr et al. 2009) has focused on the momentum in the radiation field, but we know of no work that has allowed for the momentum associated with mechanical energy emitted during AGN activity. This is curious since in the parallel case of feedback associated with star formation it is normally assumed that the momentum term dominates. But, as we noted in Paper I, the consequence of the conservation equations can be that much of the inflowing mass flows out again in the nuclear wind so that the actual ratio of the SMBH accretion $\dot{M}_{\rm BH}$ to the rate of inflowing mass ($\dot{M}_{\rm inflow}$, to be identified with $\dot{M}_1^{\rm eff}$ in Paper I) is considerably less than unity. In fact, from Equations (14) and (22) in Paper I (see also Ostriker et al. 2010 for a full discussion) it is easy to show that the ratio is

$$\frac{\dot{M}_{\rm BH}}{\dot{M}_{\rm inflow}} = \frac{1}{1+\beta}, \qquad \beta = \frac{2\epsilon_{\rm w}c^2}{v_{\rm w}^2}, \quad (3)$$

where $v_{\rm w} \simeq 10^4$ km s^{-1} is the BLR wind velocity (for simplicity here we neglect star formation in the circumnuclear accretion disk and we assume stationarity). For the low efficiency models which we will later find most appropriate ($B2_{02}$ and $B3_{02}$ in Section 4), the ratio of the mass rates is roughly between 0.6 and 0.8. But for the typical parameters used in the above quoted papers (i.e., $\epsilon_{\rm w} \sim 0.005$) this ratio can be $\simeq$0.1 so that very little mass is actually accreted on the SMBH if the calculation is done consistently. As Paper I details, we allow for all three input components (energy, momentum, and mass). In a subsequent paper, we will show how omission of one or the other of these can greatly affect results.

In the analysis of the numerical outputs, in addition to the time-averaged quantities introduced in previous papers, i.e., the accretion-weighted electromagnetic and mechanical efficiencies $\langle\epsilon_{\rm EM}\rangle$ and $\langle\epsilon_{\rm w}\rangle$ (Paper I, Equation (33)), the luminosity-weighted nuclear wind opening angle $\langle\Delta\Omega_{\rm w}\rangle$ (normalized to the total solid angle, and restricted to the phases of the model evolution when $L_{\rm BH} > 0.1L_{\rm Edd}$, Paper I, Equation (34)), and finally to the luminosity-weighted duty-cycle $f_{\rm duty}$ (Paper I, Equation (35)), we now also compute the *number of bursts* of each model (each burst being counted when $L_{\rm BH}$ becomes larger than $L_{\rm Edd}/30$) and the total time spent at $L_{\rm BH} \geqslant L_{\rm Edd}/30$ (bolometric). For selected models we also compute the number of bursts and the total time spent at $L_{\rm BH,UV}^{\rm eff} \geqslant 0.2L_{\rm Edd}/30$ (UV, after absorption), and at $L_{\rm BH,opt}^{\rm eff} \geqslant 0.1L_{\rm Edd}/30$ (optical, after absorption). The two numerical coefficients take into account the fraction of the bolometric luminosity used as a boundary condition to solve the radiative transfer equation in each of the two bands. Therefore, we can now test how well the luminosity-weighted $f_{\rm duty}$ used in our previous papers performs against the estimates of duty cycle obtained by direct number count (see Table 1). And, more importantly, we can see which, if any models show a fraction of time in the high state comparable to the fraction of black holes observed to be in an AGN phase.

We finally recall that the stellar mass loss rate and the SNIa rate associated with the initial stellar distribution are the main ingredients driving evolution of the models. In the code the stellar mass losses—the source of *fuel* for the activity of the SMBH—follow the detailed prescriptions of the stellar evolution theory, and we use exactly the same prescriptions as in CO07 (see Sections 2.2 and 2.3 therein). The radiative heating and cooling produced by the accretion luminosity are numerically computed as in CO07 by using the Sazonov et al. (2005) formulae, which describe the net heating/cooling rate per unit volume of a cosmic plasma in photoionization equilibrium with a radiation field characterized by the average quasar spectral energy distribution (SED) derived by Sazonov et al. (2004, see also Sazonov et al. 2007, 2008), whose associated spectral temperature is $T_{\rm X} \simeq 2$ keV. In particular, Compton heating and cooling, bremsstrahlung losses, and line and continuum heating and cooling, are taken into account. Also the star formation over the galaxy body, the radiation pressure due to electron scattering, to photoionization, and finally to UV, optical and infrared photons on dust, are treated as in CO07,

[6] Note that in our approach, we also consider the additional energy produced by stellar winds and SNII explosions in the stellar component of the circumnuclear disk, as apparent from Equation (20) in Paper I.

Table 1
Properties of Computed Models

Model (1)	$\epsilon_{\rm w}^{\rm M}$ (2)	$\langle\epsilon_{\rm w}\rangle$ (3)	$\langle\epsilon_{\rm j}\rangle^{\rm a}$ (4)	$\langle\epsilon_{\rm EM}\rangle$ (5)	$\log\Delta M_{\rm BH}$ (6)	$\log\Delta M_{*}$ (7)	$\log\Delta M_{\rm w}$ (8)	$\log M_{\rm gas}$ (9)	$\log l_{\rm BH,opt}^{\rm eff}$ (10)	$\log L_{\rm X,ISM}$ (11)	$\langle\Delta\Omega_{\rm w}\rangle$ (12)	$N_{\rm b}$ (13)	$\Delta t_{\rm b}$ (14)
A0	5×10^{-3}	5×10^{-3}	1.2×10^{-2}	0.003	7.17	6.43	10.38	7.65	−7.71	36.64	···	0	0
A1	2.5×10^{-4}	2.5×10^{-4}	4.4×10^{-3}	0.053	7.74	9.70	10.34	9.05	−7.59	39.13	0.5	9	32.2
A2	10^{-4}	10^{-4}	2.95×10^{-3}	0.062	7.97	9.80	10.28	9.67	−7.59	40.16	0.5	18	65.0
A3	5×10^{-5}	5×10^{-5}	1.04×10^{-3}	0.078	8.48	10.21	10.34	9.44	−7.79	39.73	0.5	23	269.5
B0	5×10^{-3}	6.3×10^{-5}	3.3×10^{-3}	0.043	8.82	9.76	10.26	9.72	−5.67	40.37	0.066	5	90.6
B1	2.5×10^{-3}	4.3×10^{-5}	3.2×10^{-3}	0.047	8.87	9.78	10.29	9.64	−5.77	40.16	0.069	6	122.5
B2	10^{-3}	2.3×10^{-5}	2.9×10^{-3}	0.052	8.96	9.84	10.34	9.44	−5.96	39.78	0.077	12	205.0
B3	3×10^{-4}	1.3×10^{-5}	2.1×10^{-3}	0.062	9.25	10.20	10.38	9.32	−6.05	39.62	0.108	27	391.1
$\mathbf{B0}_{02}$	5×10^{-3}	3.9×10^{-5}	2.1×10^{-3}	0.090	8.62	9.49	10.28	9.68	−5.21	40.21	0.066	1	36.9
$\mathbf{B1}_{02}$	2.5×10^{-3}	4.2×10^{-5}	1.6×10^{-3}	0.105	8.75	9.83	10.32	9.27	−5.44	39.54	0.074	6	132.1
$\mathbf{B2}_{02}$	10^{-3}	2.0×10^{-5}	1.9×10^{-3}	0.105	8.77	9.74	10.27	9.68	−5.13	40.23	0.093	5	172.8
$\mathbf{B3}_{02}$	3×10^{-4}	1.2×10^{-5}	1.2×10^{-3}	0.133	9.06	10.22	10.31	9.34	−5.43	39.63	0.080	22	600.0
$\mathbf{B0}^{\mathbf{w}}$	5×10^{-3}	4.8×10^{-5}	5.0×10^{-3}	0.028	8.55	9.41	10.31	9.50	−5.79	39.94	0.172	93	16.1
$\mathbf{B1}^{\mathbf{w}}$	2.5×10^{-3}	2.4×10^{-5}	4.7×10^{-3}	0.029	8.64	9.40	10.25	9.74	−5.41	40.60	0.150	64	18.2
$\mathbf{B2}^{\mathbf{w}}$	10^{-3}	2.0×10^{-5}	2.5×10^{-3}	0.047	8.91	10.21	10.35	9.36	−5.97	39.68	0.176	192	67.5
$\mathbf{B3}^{\mathbf{w}}$	3×10^{-4}	6.5×10^{-6}	2.6×10^{-3}	0.047	9.04	10.18	10.32	9.66	−5.79	40.15	0.241	120	95.0
$\mathbf{B0}^{\mathbf{w}}_{02}$	5×10^{-3}	6.9×10^{-5}	3.3×10^{-3}	0.068	8.35	8.97	10.33	9.37	−5.25	39.65	0.208	46	13.7
$\mathbf{B1}^{\mathbf{w}}_{02}$	2.5×10^{-3}	4.0×10^{-5}	2.8×10^{-3}	0.074	8.44	9.04	10.32	9.46	−5.21	39.84	0.242	31	12.9
$\mathbf{B2}^{\mathbf{w}}_{02}$	10^{-3}	2.9×10^{-5}	2.1×10^{-3}	0.093	8.64	9.87	10.32	9.52	−5.22	39.91	0.266	73	67.1
$\mathbf{B3}^{\mathbf{w}}_{02}$	3×10^{-4}	4.9×10^{-6}	1.7×10^{-3}	0.111	8.89	10.36	10.33	9.57	−5.26	40.03	0.077	102	423.6

Notes. Masses are in units of solar masses and luminosities in erg s^{-1}. In Type A models the nuclear wind efficiency is maintained constant, i.e., $\epsilon_{\rm w}=\epsilon_{\rm w}^{\rm M}$, while in Type B models the value $\epsilon_{\rm w}^{\rm M}$ is reached when $L_{\rm BH}\geqslant 2L_{\rm Edd}$ (Equation (6)). In models with the subscript 02 the maximum radiative efficiency is $\epsilon_0=0.2$ instead of 0.1 (Equation (1)). Mass-accretion-weighted efficiencies in Columns (3)–(5) are calculated according to Equation (34) in Paper I. ΔM_* is the total amount of star formed during the model evolution, $\Delta M_{\rm w}$ is the total amount of ISM lost at $10R_{\rm e}$ and $M_{\rm gas}$ the instantaneous amount of gas inside $10R_{\rm e}$. The scaled luminosity $l_{\rm BH,opt}^{\rm eff}=L_{\rm BH,opt}^{\rm eff}/L_{\rm Edd}$ in Column (10) is the Eddington normalized SMBH luminosity in the optical as would be seen at infinity after absorption, with $L_{\rm BH,opt}^{\rm eff}=0.1L_{\rm BH}$ at the first grid point (see CO07 for details). Column (12) lists the luminosity-weighted solid opening angle of each of the two BLR wind conical regions (normalized to half solid angle). In model A0 no value is provided, as the nuclear luminosity never exceeds the limit $L_{\rm Edd}/10$. Finally, in Columns (13) and (14) we give the total number of bursts and the total time (in Myr) spent by the SMBH at (bolometric) $L_{\rm BH}\geqslant L_{\rm Edd}/30$.

[a] Figures corresponding to quantities calculated but not added to the hydrodynamical equations.

where the derivation and the numerical integration scheme of the radiative transport equations is described in detail. All the relevant information about the one-dimensional numerical code and the hydrodynamical equations can be found in Ciotti & Ostriker (2001) and CO07.

3. COMBINED MODELS WITH FIXED MECHANICAL EFFICIENCY

In order to better follow the description of the results of the new simulations, here we summarize the principal phases of the model evolution as produced by the numerical simulations. These main aspects are almost independent of the specific modelization of the mechanical feedback treatment, and so apply also to the models in Section 4.

Overall, we found that in combined models the main properties of model evolution are preserved; in particular, episodic outbursts reaching $0.1L_{\rm Edd}$ can be common. After a first evolutionary phase in which a galactic wind is sustained by the combined heating of SNIa and thermalization of stellar velocity dispersion, the central "cooling catastrophe" of the galaxy gaseous halo commences, with the formation of a collapsing cold shell at ∼1 kpc from the center. In the absence of the feedback from the central SMBH a "mini-inflow" would then be established, with the flow stagnation radius (i.e., the radius at which the flow velocity is zero) of the order of a few hundred pc to a few kpc: these decoupled flows are a specific feature of cuspy galaxy models with moderate SNIa heating (Pellegrini & Ciotti 1998). After the cooling catastrophe, the SMBH feedback affects the subsequent evolution, and the number of bursts depends on the nature and strength of the feedback. Nuclear bursts are accompanied by significant episodes of star formation in the central regions of the galaxy, and obscuration of the nuclear source can be considerable. As already found in CO07, the major AGN outbursts are separated by increasing intervals of time (set by the cooling time and by the secular decrease of the mass return rate from the evolving stellar population), and present a characteristic temporal substructure, whose origin is due to the cooperating effect of direct and reflected shock waves (from the inner rim of the spherical strongly perturbed zone). In general, purely mechanical feedback tends to produce "clean" bursts, while radiative feedback leads to bursts consisting of several sub-bursts. In all cases, these outflowing shocks are a likely place to produce emission of synchrotron radiation and electron and ionic cosmic rays (see Jiang et al. 2010, see also Sijacki et al. 2008). Finally, at late epochs the galaxy models are usually found in a state of stationary, very sub-Eddington hot accretion, in an ADAF state.

We now illustrate the results obtained in the combined models, starting with the description of the simplest combined models, designated by "A" in Paper I. These A models should be compared with the corresponding purely mechanical MA models in Papers I (Table 2) and II, in order to determine the additional effects of radiative feedback; in fact MA models were

meant to investigate the effects of mechanical feedback, so that radiative effects were excluded from the simulations. Type A models adopt the commonly assumed prescription of a fixed mechanical efficiency for the nuclear wind, i.e., in Equation (2)

$$\epsilon_{\rm w} = \epsilon_{\rm w}^{\rm M}, \tag{4}$$

where $\epsilon_{\rm w}^{\rm M}$ is the value reported in Column 2 of Table 1. From Equation (2) it follows that the mechanical energy flowing out of the central SMBH regions bears a fixed relation to the mass accreted by the SMBH. This is what is normally assumed in works on AGN feedback (e.g., Di Matteo et al. 2005; Johansson et al. 2008). Therefore, for the A models the mass-accretion-weighted nuclear wind efficiency $\langle\epsilon_{\rm w}\rangle$ (Equation (33) in Paper I), coincides with $\epsilon_{\rm w}^{\rm M}$, as apparent from Column 3 of Table 1. It is important to stress, however, that in the simulations only a fraction of the mechanical energy is transferred to the interstellar medium (ISM), and at different radial scales, as described by the physically based differential Equation (29) derived and discussed in detail in Paper I. In all the presented models A0–A3, the mass ejected with the nuclear wind (that would be observed as a BLR wind), is a factor of 2 greater than the mass accreted on the central SMBH, and the nuclear wind opening angle is maintained fixed, i.e.

$$\eta_{\rm w} = 2, \quad \Delta\Omega_{\rm w} = \pi, \tag{5}$$

(see Equations (17), (18), and (31) in Paper I). Finally, the maximum radiative efficiency ϵ_0 in Equation (1) adopted in the four A models presented in Table 1 is fixed to 0.1: note how the implemented ADAF-like treatment, leads to the reduced accretion-mass-weighted values for $\langle\epsilon_{\rm EM}\rangle$, as reported in Column 5.

The model results are given in Table 1 in the order of decreasing mechanical efficiency $\epsilon_{\rm w}^{\rm M}$ (Column 2), with the first model A0 adopting the conventionally chosen constant mechanical efficiency of 0.005; a direct comparison with the results of the correspondent purely mechanical models MA0–MA3 can be done by inspecting Table 2 in Paper I. As expected, reducing the wind mechanical efficiency increases the SMBH accretion rate, and so the emitted luminosity increases, as apparent from the values in Columns 5 and 6. Column 7, where we list the total stellar mass of the new stars, confirming a previous finding of our models: in practice, also in the combined models, *a larger number of AGN bursts (consequence of a reduction of the mechanical feedback efficiency), leads to a larger amount of star formation*. In addition, the final mass of new stars is (slightly) larger than in the purely mechanical MA models, due to the fact—already described in Paper I—that a single burst in the presence of radiative feedback tends to be richer in the temporal substructure, leading to a longer period of nuclear star formation activity. Therefore we again confirm that, while it is believed that in the process of galaxy formation the feedback from the central SMBH may help to end the galaxy formation epoch, in the successive (and unavoidable) evolution driven by the mass return from the evolving stars, AGN feedback may actually lead to an increase of star formation, in the inner few hundred parsecs of the galaxy. As described in CO07, this phenomenon can lead to a build-up of a stellar "cusp" of new stars at the center of galaxies experiencing repeated AGN bursts, with structural properties in nice agreement with observational findings. We will return more extensively to this point in Section 4.2.

As noted in Section 2, the model with the "standard" high efficiency, A0, requires such a large fraction of the inflowing mass to be returned in the outflowing wind that very little accretes onto the central SMBH. As a consequence its mass increases by only $\sim 10^7\,M_\odot$ (Table 1, Column 6), and the observed $M_{\rm BH}$–σ relation could certainly not be maintained by this type of model. In addition, the final thermal X-ray luminosity would be too low.

Remarkably, the time integral of the gas lost by the galaxy at 10 $R_{\rm e}$ (Column 8), does not depend strongly on the assumed value of mechanical feedback efficiency, as it is mainly driven by SNIa heating. Actually, a *decrease* of the mechanical wind efficiency produces a slightly larger degassing, a consequence of the increased number of bursts. The combined effect of SMBH accretion, galaxy degassing, and star formation is the explanation of the non-monotonic behavior of the present-day amount of hot, X-ray emitting gas in the galaxy (Column 9): for very high efficiencies (model A0) the gas mass is very low, so that the X-ray luminosity is also correspondingly low (Column 11). At very low mechanical efficiencies (model A3), a significant amount of gas has been accreted on the SMBH but, most importantly, the considerable star formation induced by the repeated bursts deprives the galaxy of gas; for intermediate values of mechanical efficiency (model A2) the amount of hot gas is maximized, and the X-ray luminosity also reaches a present-day value consistent with X-ray emitting galaxies. As already stressed in Section 1, we again recall that pressure from the ICM will increase the luminosity values. In summary, matching the models and the observed X-ray thermal luminosity is a sensitive constraint. Both too little or too much feedback deprives the galaxy of gas and reduces the X-ray output to values below what is observed.

In Column 10, we list the present-day SMBH luminosity, measured in units of Eddington luminosity: the main reason for the decline at decreasing mechanical efficiency is the substantial increase in the final SMBH mass. In Column 13, we report the number of bursts of the model. We count as a burst every time the bolometric accretion luminosity grows above the fiducial limit of $L_{\rm Edd}/30$, and in Column 14 we report the total time (in Myr) spent by the bolometric accretion luminosity above the threshold of $L_{\rm Edd}/30$. As already described, the number of bursts increases with decreasing mechanical efficiency, and also the average duration of each burst, going from $\approx$4 Myr in model A1 up to $\approx$12 Myr in model A3. These results are in nice agreement with observational estimates (e.g., Kirkman & Tytler 2008). *It is important to stress that the obtained time scales for the nuclear bursts are not imposed, but are self-determined by the evolutionary physics*: in addition, several sub-bursts are in general grouped in a time extended single burst, following the physics described in CO07 and in Paper I.

For example, the nine bursts counted in model A1 are just the temporal substructure of the single burst appearing in Figure 2 (left panels). In this model after one large burst most of the ISM in the galaxy is expelled and there is little further activity. This is similar to what Di Matteo et al. (2005) found, and has some attractive features in showing the power possible from AGN feedback, but, as noted above, very little mass will be accreted on the central SMBH in this type of model if mass conservation is strictly enforced. The evolution of model A2, with a reduction of the mechanical efficiency by a factor of 2.5 is also shown in Figure 2 (right panels). The most evident and expected feature is the increase in the number of bursts.

Are these models (A1 and A2) an adequate representation of reality? Was the addition of radiative feedback able to cure some of the problems affecting the purely mechanical MA models

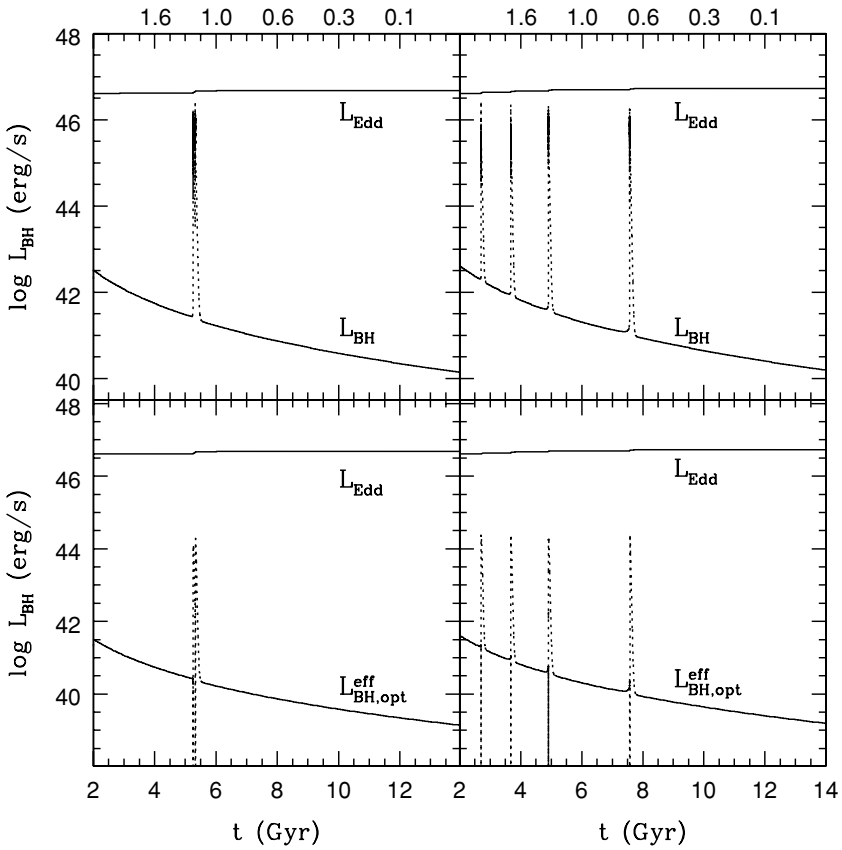

Figure 2. Luminosity evolution of model A1 (left panels), a model with constant mechanical efficiency $\epsilon_{\rm w} = 2.5 \times 10^{-4}$ and also radiative feedback. After one large burst the gas reservoir in the galaxy is so depleted that no further bursts occur. Same quantities for model A2 (right panels), in which $\epsilon_{\rm w} = 10^{-4}$. Dotted lines are the bolometric accretion luminosity (top) and the optical SMBH luminosity corrected for absorption, i.e., as it would be observed from infinity (bottom). As in CO07 at the center we fixed $L^{\rm eff}_{\rm BH,opt}(R_1) = 0.1 L_{\rm BH}$. The global properties of the models are given in Table 1. In the top horizontal scale of this and of all the other figures the redshift corresponds to the bottom time scale.

described in Papers I and II? We think that they are not. In fact, there are two salient defects. First the final gas luminosity and the final gas mass are both below those typically seen in elliptical galaxies (Pellegrini et al. 2009; Diehl & Statler 2007). Second, as noted, the central SMBH accretes very little mass. The reason for the much lower accretion found here than in other works (e.g., Di Matteo et al. 2005) is in part that the latter have assumed an accretion rate of 100 times the Bondi rate, whereas we have computed the accretion rate self-consistently (see also a discussion of this issue in Kurosawa et al. 2009, and Figure 1 therein); and in addition the outward mass flow has not been, in general, incorporated in the calculation. In any case this high assumed wind efficiency seems to lead to results in conflict with well-established observations, so we have rescaled to lower values the assumed wind efficiency in model A3, keeping the peak radiative efficiency at 0.1, and the mechanical efficiency constant. In conclusion, it does not appear that low-efficiency models will be satisfactory for any adopted value of the mechanical efficiency. The reason is that the energy input is restricted to a region very near the central SMBH and that models with sufficiently low efficiency to grow reasonable size SMBHs have so little energy input into the bulk of the galaxy that cooling-flow-induced starbursts leave the galaxy with too much gas and too high rates of central star formation. Also, very low efficiency models would leave most ellipticals with an E+A spectrum seen in the central regions due to recurrent starbursts (e.g., see Wang et al. 2009, see also Paper II).

4. COMBINED MODELS WITH LUMINOSITY-DEPENDENT MECHANICAL EFFICIENCY

On the basis of the previous investigation, we are now in the position to explore a family of models (type B models) in which the amount of gas ejected by the nuclear wind, the mechanical wind efficiency, and the wind opening angle depend on the Eddington normalized bolometric accretion luminosity $l = L_{\rm BH}/L_{\rm Edd}$ as

$$\eta_{\rm w} = \frac{3\eta^{\rm M}_{\rm w}}{4}\frac{l}{1+0.25\,l}, \quad \epsilon_{\rm w} = \frac{3\epsilon^{\rm M}_{\rm w}}{4}\frac{l}{1+0.25\,l},$$
$$\Delta\Omega_{\rm w} = \pi\,\min(\sqrt{l^2+a^2}, 1), \tag{6}$$

where $a = 2.5 \times 10^{-2}/\pi$ (Paper I, Equations (18), (21), (31); and Figure 1 therein). In order to have a velocity of nuclear winds with observed values we must assume $\eta^{\rm M}_{\rm w} \simeq 1800\epsilon^{\rm M}_{\rm w}$, in accordance with the relation

$$v_{\rm w} \simeq \sqrt{\frac{2\epsilon_{\rm w}}{\eta_{\rm w}}}\,c \approx 10^4\,{\rm km\,s^{-1}}. \tag{7}$$

These assumptions, while somewhat different from those normally made by galaxy modelers, are closer to what is expected from studies of central engines (e.g., Proga et al. 2000; Proga & Kallman 2004; Benson & Babul 2009), and possibly with

observational evidences (Allen et al. 2006). In particular, wind efficiency and ejected mass fraction increase at increasing l and saturate at $l \geqslant 2$ at the values $\epsilon_{\rm w}^{\rm M}$ and $\eta_{\rm w}^{\rm M}$; the wind (solid) opening angle also increases for increasing l, in the range 2.5×10^{-2} to π. As in the case of the combined A models, in the combined B models we also consider both mechanical and radiative feedback, adopting the ADAF prescription (1). However, we now explore two families of radiative efficiencies: in the first (analogous to the A models presented in the previous section) $\epsilon_0 = 0.1$, while in the second (the B_{02} models in Table 1) the peak EM efficiency is increased to $\epsilon_0 = 0.2$. Again, as for the A models, the explicit time-dependent term in the differential equation describing the discharge of the nuclear wind mass, momentum, and kinetic energy on the galaxy ISM (Paper I, Equation (29)), is not taken into account. This further ingredient is activated in the suite of $B^{\rm w}$ models, briefly described in the following section.

We start by considering the overall properties of the combined B models with $\epsilon_0 = 0.1$ (B0–B3 in Table 1), ordered for decreasing $\epsilon_{\rm w}^{\rm M}$. A few systematic behaviors can be easily spotted. For example, as for the A models, the mass-accretion-weighted mechanical efficiency $\langle\epsilon_{\rm w}\rangle$ (Table 1, Column 3) decreases moving from model B0 to model B3, a direct consequence of the reduction in the adopted value for the peak mechanical efficiency $\epsilon_{\rm w}^{\rm M}$. Also, the mass-accretion-weighted EM efficiency $\langle\epsilon_{\rm EM}\rangle$ increases at decreasing $\epsilon_{\rm w}^{\rm M}$, due to the increasing number of burst events, and so of high-luminosity peaks (Column 13). The total mass accreted by the SMBH, $\Delta M_{\rm BH}$, as expected increases from model B0 to model B3. However, the variation of $\Delta M_{\rm BH}$ for different values of $\epsilon_{\rm w}^{\rm M}$ is smaller than in the A family. In general, for similar values of $\epsilon_{\rm w}^{\rm M}$, the accreted mass in B models is larger than in A models: this difference is due to the fact that in B models, between two successive bursts, the mechanical feedback drops because the solid opening angle decreases to values corresponding to a classical jet, and the mechanical efficiency drops virtually to zero. This is not a minor effect, and it shows how a non-negligible amount of mass is also accreted in the low-luminosity phases between bursts. The amount of star formation also increases at decreasing $\epsilon_{\rm w}^{\rm M}$, as for the family of A models (Table 1, Column 7). But, as for the total mass accreted on the SMBH, also for the mass in new stars, B models accumulate significantly larger masses, with final $\Delta M_* \gtrsim 10^9\ M_\odot$ in B0, up to $10^{10}\ M_\odot$ in model B3.

The additional effect of radiative feedback on the models with a luminosity-dependent mechanical feedback can be determined by comparison of the present results with those of purely mechanical MB models listed in Table 2 of Paper I. Here we just notice how the final SMBH masses in combined models are in better agreement with observational values, where purely mechanical (and the purely radiative RB models, also presented in Table 2 of Paper I) models tend to produce too large SMBHs. This fact clearly points out the importance of the cooperation of mechanical and radiative feedback in self-regulating galaxy evolution. This point will be discussed on more physical grounds in Section 4.2. The effects of an increase of the peak value of radiative efficiency in combined models (from 0.1 to 0.2) are shown by the B_{02} family in Table 1. All the trends with $\epsilon_{\rm w}^{\rm M}$ are similar to models with $\epsilon_0 = 0.1$, but the final SMBH masses slightly reduced, as expected.

Overall, we can summarize the main results of this section as follows. It is apparent that the combined B models behave better than the combined A models, in the sense that mechanical feedback is sufficiently strong to add its effects to radiative feedback, but it is not so strong as to prevent the recurrent cooling catastrophe events, so that the galaxy is not in a permanent wind state, and contains sufficient gas to produce substantial coronal X-ray luminosity. In the case of very low assumed efficiency for wind input, of course the global evolution is similar to that of purely radiative models, while in the case of high efficiency the evolution is significantly different. Motivated by the encouraging results of the combined B family, in the following section we focus our attention on two B models that account most satisfactorily for several observational properties. We recall that details of X-ray properties of these models (such as their surface brightness in the soft and hard bands used in observational works, and luminosity-weighted X-ray temperatures during the different evolutionary phases) have been already presented elsewhere (Pellegrini et al. 2009).

4.1. Representative "Best" Models

The two "best" models among those we have studied are $B2_{02}(\epsilon_{\rm w}^{\rm M} = 10^{-3})$ and $B3_{02}(\epsilon_{\rm w}^{\rm M} = 3 \times 10^{-4})$, with peak mechanical efficiencies in agreement with observational values (Schlesinger et al. 2009). These will be considered our fiducial models bracketing the optimal values for the input parameters and for output quantities. Each of the two has interesting properties that we now discuss in some detail, beginning with a discussion of the time evolution of luminosities and mass accretion rates.

The luminosity evolution of the two models is shown in Figure 3. From comparison of the left and right panels, it is apparent how a reduction in the peak value of mechanical efficiency affects the time evolution, number, and temporal structure of the bursts. Since the mechanical efficiency in model $B2_{02}$ is three times higher than in model $B3_{02}$, the number of bursts in the former is 3, while in the second 4; moreover, as is common in radiative feedback models (see also Paper I) each single burst is organized in several sub-bursts. We note that the central optical/UV luminosities are far below the Eddington limit (5 orders of magnitude!) at the current epoch in these fiducial models in rough agreement with current observations (e.g., see Pellegrini 2005; Ho 2009). However, we find that even at these accretion rates the mechanical and radiative feedback are sufficiently strong to heat gas near the SMBH to the level when the numerical self-consistently calculated "Bondi-rate" is very low.

This luminosity evolution corresponds to the different mass accretion (and ejection) histories, as plotted in Figures 4 and 5. In fact, the final SMBH mass and mass of the new stars added to the galaxy is $\Delta M_{\rm BH} \simeq 5.9 \times 10^8\ M_\odot$ and $\Delta M_* \simeq 5.5 \times 10^9\ M_\odot$ in model $B2_{02}$, while for the model $B3_{02}$ the same quantities are $\simeq 1.1 \times 10^9\ M_\odot$ and $\simeq 1.7 \times 10^{10}\ M_\odot$, respectively (see Table 1). The ejected mass as a galactic wind is very similar in both cases, summing up to $\simeq 2 \times 10^{10}\ M_\odot$ of material. The star formation rate during the periods of feedback-dominated accretion oscillates from 0.1 up to several hundreds (with peaks near 10^3) $M_\odot\ {\rm yr}^{-1}$ (the ULIRGs level), while it drops monotonically to $\lesssim 10^{-1}\ M_\odot\ {\rm yr}^{-1}$ in the last 6 Gyr of quiescent accretion in model $B2_{02}$ (Figure 4, red line, bottom panel), and to $\sim 3 \times 10^{-2}\ M_\odot\ {\rm yr}^{-1}$ in the last 4 Gyr in model $B3_{02}$ (Figure 5), consistently with observations of star formation signatures in optically quiescent early-type galaxies (e.g., Salim & Rich 2010). It is also apparent how the star formation episodes are on one side enhanced by SMBH feedback, but also how they end abruptly after major SMBH outbursts (e.g., see Schawinski et al. 2009; Nesvadba et al. 2010).

The temporal evolution of the integrated luminosities of other mass components of the models clearly reflects the accretion his-

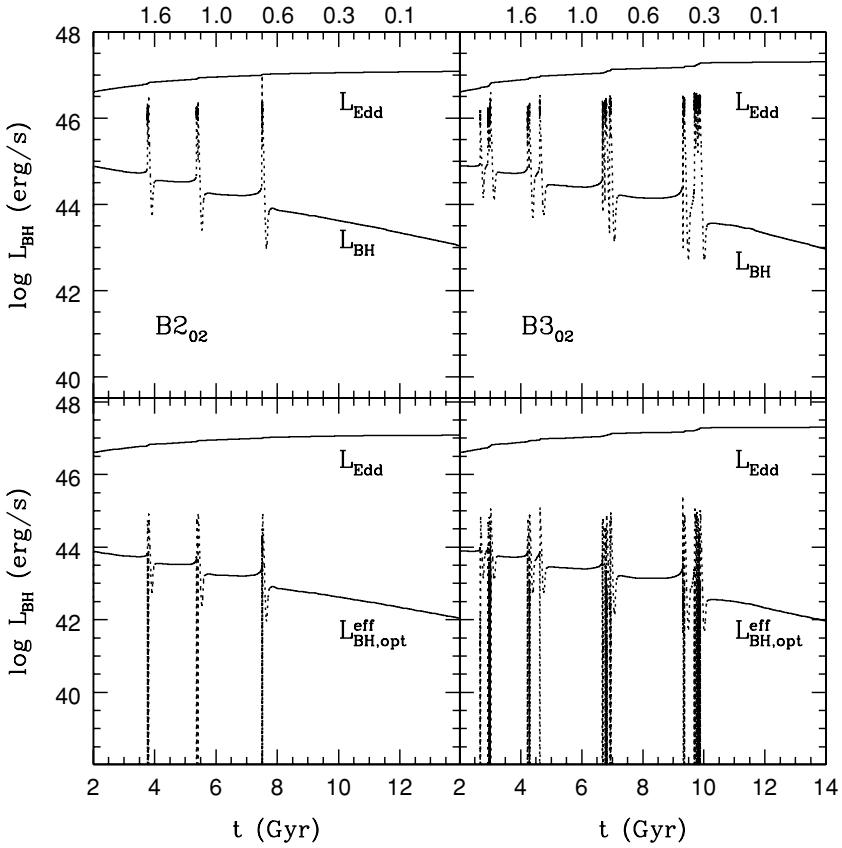

Figure 3. Fiducial models showing evolution of SMBH luminosity. Luminosity evolution of model $B2_{02}$ (left panels), a model with peak mechanical efficiency $\epsilon_{\rm w}^{\rm M} = 10^{-3}$ and also radiative feedback. Same quantities for model $B3_{02}$ (right panels), in which $\epsilon_{\rm w}^{\rm M} = 3 \times 10^{-4}$. Dotted lines are the bolometric accretion luminosity (top) and the optical SMBH luminosity corrected for absorption, i.e., as it would be observed from infinity (bottom). The global properties of the models are given in Table 1. Note that at the current epoch ($z = 0$) the SMBH bolometric luminosity $L_{\rm BH}$ is 4 orders of magnitude below the Eddington limit $L_{\rm Edd}$.

tory, as shown in Figure 6. In panels (a) and (b) we show the evolution of the X-ray luminosity of the hot galaxy atmosphere, integrated within $10R_{\rm e}$. The sharp peaks are due to sudden increases in the X-ray surface brightness profiles in the central regions, a consequence of AGN feedback. During more quiescent phases, L_X attains values comparable to the observed ones, and it is expected that a central galaxy will reach higher values, due to confining effects of the ICM. On the contrary, stripping effects of the ICM in satellite galaxies lead to a further reduction (see Shin et al. 2010b). In panels (c) and (d), we show the reprocessed IR radiation from the central starbursts and the associated SMBH accretion, with peak values similar to those observed in ULIRGs (e.g., see Nardini et al. 2010). We note that peaks of nuclear IR emission coupled with nuclear radio/X-ray emission have been recently reported in a sample of elliptical galaxies (Tang et al. 2009); the authors suggest that the correlation indicates that the excess IR emission is related to nuclear activity, and presumably due to hot dust heated by the central AGN. Finally, in panels (e) and (f) the luminosity of the starburst in the UV and optical, after correction for absorption (i.e., as would be seen from infinity, as described in CO07) is shown. It is apparent how a large fraction of the starburst luminosity output occurs during phases when shrouding by dust is significant (e.g., Rodighiero et al. 2007; Brusa et al. 2009), i.e., the model would be observed as an IR source with UV and optical in the range seen in brighter E+A sources. Opacity effects are also apparent in the rise of the two luminosities in model $B3_{02}$ at late times, due to a substantial decrease in the ISM opacity associated with the degassing of the galaxy central regions consequent to the last major burst around 10 Gyr. Of course, due to the longer time scales of star formation, the peaks of the UV and optical light curves are less sharp than those relative to SMBH luminosity; we notice that the measure of the different time scales of nuclear accretion and associated star formation can now be measured, with very interesting results (Wild et al. 2010).

As anticipated, at variance with our previous papers, we compute here the duty cycle as the total time spent by the AGN at high-luminosity phases, normalized to the age of the system at the specified time, while in our previous papers we adopted a luminosity-weighted definition. The new duty-cycle values (at the current epoch) are just obtained by dividing the figures in Column 14 of Table 1 by the total time spent by the simulation, i.e., 12.5 Gyr. In other words, we estimate the observable duty cycle as the fraction of the total time that the AGN is in the "on" state. We found that the average values are very similar to the luminosity-weighted values, but here we prefer to use the new approach, as its interpretation is more direct (the older one depending also on the adopted time-fraction of the total time interval over which backward integration is done). The results in different wavebands (namely, optical and UV after absorption, and bolometric) are presented in Figure 7: as expected, at each time the larger duty cycles are in the bolometric, followed by (absorbed) optical and finally by absorbed UV. For example, for the two best models the total time spent at high luminosity in optical is in the range 130–380 Myr. The bolometric values obtained from Table 1 are comparable (even though slightly larger) than the duty cycles computed according to the luminosity-weighted recipe adopted in CO07 and in

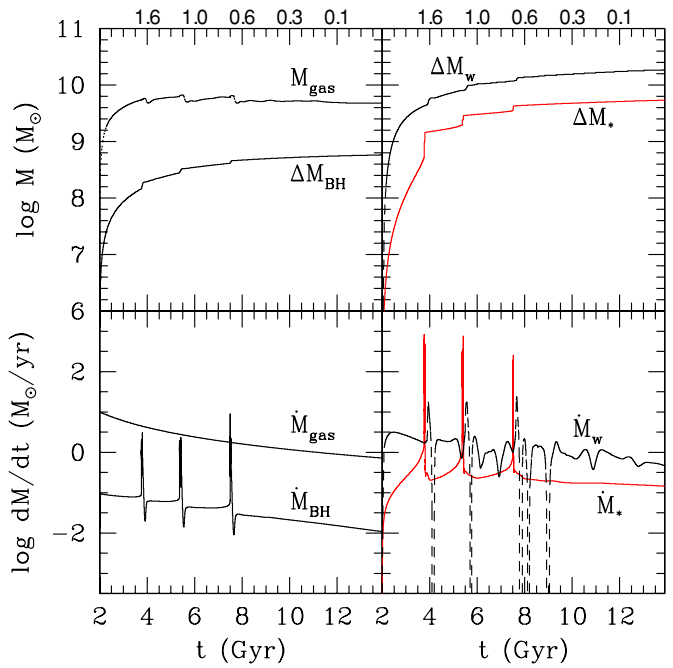

Figure 4. Mass budget evolution of model $B2_{02}$. Top left panel: mass accreted on the central SMBH and ISM mass inside $10R_e$. Top right: total mass of gas ejected from the galaxy at $10R_e$, and total mass of new stars in the galaxy. In the bottom panels the corresponding rates are shown. The bulk ($\simeq$63%) of the recycled gas is ejected in galactic winds, with $\simeq$19% of it converted to centrally located stars, $\simeq$2% of it accreted to the central SMBH, and finally $\simeq$16% of it under the form of X-ray emitting hot ISM. Note that in the pulsed activity of bursts the wind ejection rate from the galaxy can exceed 100 $M_\odot$ yr^{-1}, and also how peaks in the star formation anticipate the large degassing events.

(A color version of this figure is available in the online journal.)

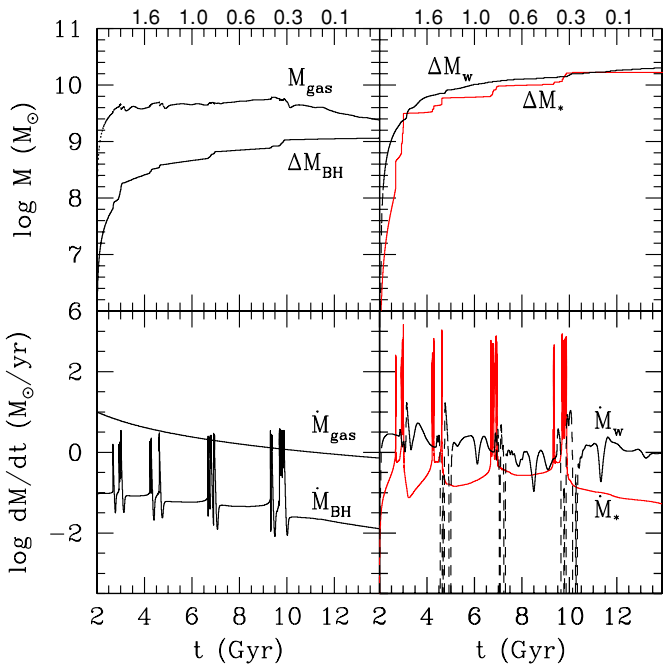

Figure 5. Mass budget evolution of model $B3_{02}$. Panels and lines as in Figure 4. Behavior is essentially similar but the weaker mechanical feedback permits bursts to last till later cosmic time. The frequency and intensity of mass expulsion and star formation events is paradoxically greater for lower mechanical efficiency.

(A color version of this figure is available in the online journal.)

Paper I. For example, we see that model $B3_{02}$ has a bolometric duty cycle of $\simeq$5%, while in the absorbed UV the duty cycle drops to $\simeq$2%.

Of course, these values (by construction) cannot take into account the temporal decline of the accretion activity over the Hubble time. As an experiment, we considered the duty cycle obtained by starting the analysis at 6 and at 9 Gyr. The resulting numbers are significantly smaller: for example, in model $B2_{02}$ the duty cycle is zero when starting at 9 Gyr (as no bursts occur after $\simeq$7.5 Gyr), while using 6 Gyr as the initial time we obtain $\simeq 5.2\times10^{-3}$, 2.6×10^{-3}, and 2.5×10^{-3} in bolometric, optical, and UV bands, respectively. A similar (but less strong) reduction is also presented by model $B3_{02}$, with computed duty cycles in the bolometric, optical, and UV of $\simeq(4\times10^{-2}, 1.5\times10^{-2}, 7.5\times10^{-3})$, respectively (when starting the count at 6 Gyr), and of $\simeq(3.6\times10^{-2}, 1.3\times10^{-2},$ and $5.2\times10^{-3})$ (when starting the count at 9 Gyr). These values compare nicely with observational estimates (e.g., Heckman et al. 2004; Greene & Ho 2007).

We now focus on a remarkable observational feature of our models, already noticed in the case of purely radiative feedback models in CO07, and nicely confirmed by combined models. The violent star formation episodes associated with the recurrent nuclear accretion events (with SMBH accretion to star formation mass ratios $\sim10^{-2}$ or less) are induced by accretion feedback, and are spatially limited to the central 10–100 pc; thus, the bulk of gas flowing to the center is consumed in the starburst. These findings are nicely supported by recent observations (e.g., see Lauer et al. 2005; Davies et al. 2007, 2009; Shapiro et al. 2010). In fact, as noticed by Lauer et al. (2005), where colors and luminosities of the nuclear regions of elliptical galaxies are studied, on average the "nuclear" clusters are bluer than the surrounding galaxy, and in some cases they are very well resolved at the distance of Virgo. An interesting example is the central system in NGC 4365 (Figure 3 in Lauer et al. 2005), in which a blue, extended source well interior to the core is detected.[7] Note that the "age" effect of the new stars on the global stellar population of the galaxy is small, as the new mass is only 3% of the original stellar mass, and it is virtually all accumulated during the first Gyr, so that the mass-weighted age of the final model is still of the order of 12 Gyr. The half-mass radius of the final stellar distribution (without considering adiabatic contraction, nor the reduction of the stellar mass distribution due to galactic winds, two phenomena not considered in the present simulations) remains almost unchanged in model $B2_{02}$, in accordance with the moderate amount of new stars formed (Figure 4, red line, top panel; and Table 1), while it contracts by $\sim$10% in model $B3_{02}$ (due to the larger amount of gas transformed in new stars, see Figure 5, red line, top panel; Table 1), from $R_e = 6.9$ kpc to $R_e = 6.2$ kpc. This addition of the new stars in the central regions of the galaxy is made apparent in Figure 8, where with dotted lines we show the initial (bottom panels) and spatial (top panels) projected stellar density profiles of models $B2_{02}$ and $B3_{02}$, together with their best fit (solid lines) obtained with the Sersic (1968) law

$$\Sigma(R) = \Sigma_0 e^{-b(R/R_e)^{1/m}}, \quad (8)$$

(where $b = 2m - 1/3 + 4/405m + \mathcal{O}(m^{-2})$; Ciotti & Bertin 1999). As expected, the profiles show an increase of the global best-fit Sersic parameter m from $\simeq$4.5 up to $m \simeq 6$, due to the

[7] It is interesting that small compact blue nuclear clusters are seen in many ellipticals with cores (T. Lauer 2010, private communication).

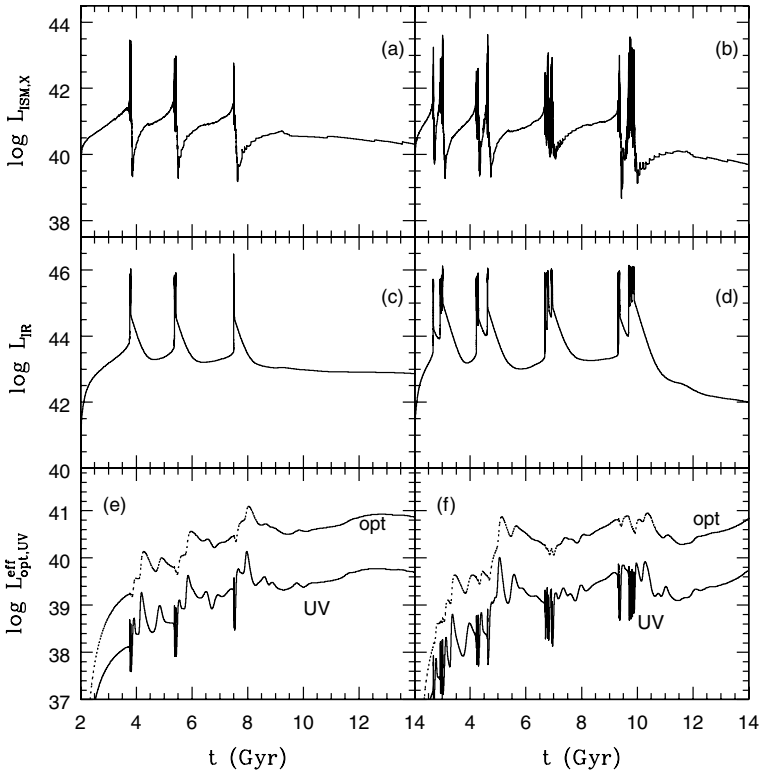

Figure 6. Time evolution of the galactic X-ray coronal luminosity L_X (top), recycled infrared luminosity L_{IR} (middle), and the starburst UV and optical luminosities (bottom), corrected for absorption. Left panels refer to model $B2_{02}$ and right panels to model $B3_{02}$. The infrared luminosity is due to the reprocessing of the radiation emitted by the new stars and by the SMBH and absorbed by the ISM inside $10R_e$ (see Equation (51) in CO07). At late times the thermal X-ray luminosity is $\sim 10^{40}$ erg s^{-1} and the post-starburst (E+A) luminosity is a fraction of a percent of the light from stars.

mass accumulation in the central regions. Remarkably, the final value of m is within the range of values commonly observed in massive ellipticals: however, in the final model we note the presence of a central ($\sim$30 pc) nucleus originated by star formation which stays above the best-fit profile, similar to the light spikes characterizing "nucleated" or "extra-light" galaxies, that are usually attributed to galaxy merging (e.g., see Hopkins et al. 2009, and references therein). Such "cuspy" ellipticals provide one of the two important branches of the elliptical galaxy sequence (e.g., see Graham 2004; Graham & Driver 2005; Lauer et al. 2005; Kormendy et al. 2009; see also Ciotti 2009b; Côté et al. 2006, 2007). Observational evidence is also accumulating that the central parts are quite metal rich (e.g., see Chilingarian et al. 2009; Lee et al. 2010; Rafanelli et al. 2010) as would be expected if the origin were from infalling gas recycled from evolving stars.

As in these models we are now considering both the effects of radiative and mechanical feedback, it is interesting to show where the bulk of feedback energy is deposited. We illustrate this in Figure 9, for three times just before (left column), near the end (central column), and after the first burst (right column) of model $B3_{02}$. For illustration, we also plot the corresponding radial profiles of gas density (top panels) and gas velocity (central panels). In the bottom panels, solid lines represent the volume-weighted profiles of radiative energy deposition, while the dotted lines show the corresponding mechanical energy deposition. A clear trend is apparent: while after and before the burst the radiative feedback affects all the galaxy volume (due to the low opacity of the hot ISM), and the mechanical feedback is concentrated in the central kpc region, during the burst almost all the AGN radiation is absorbed (and reprocessed in the IR) by the cold and optically thick collapsing shell. This means that

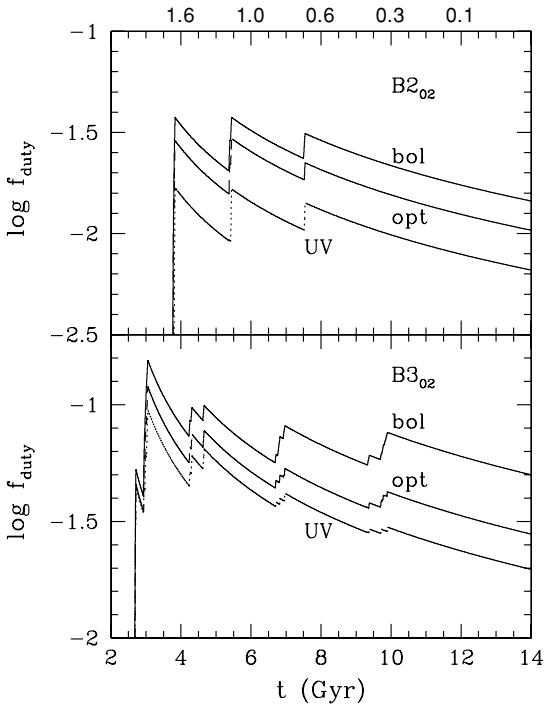

Figure 7. Time evolution of cumulative duty cycle (defined as fraction of the elapsed time during which the AGN is flaring at more than a fixed threshold) of the nucleus in the bolometric, in the absorbed (i.e., as would be seen from infinity) optical, and absorbed UV bands, for models $B2_{02}$ and $B3_{02}$. For example, in the optical band between 1% and 3% of SMBH would be seen in the "on" state at the current epoch, if using as a time baseline for the estimate the whole integration time of the simulation (see the text for a more detailed explanation). The scale at the top indicates the redshift in a flat universe corresponding to the age in the abscissa axis.

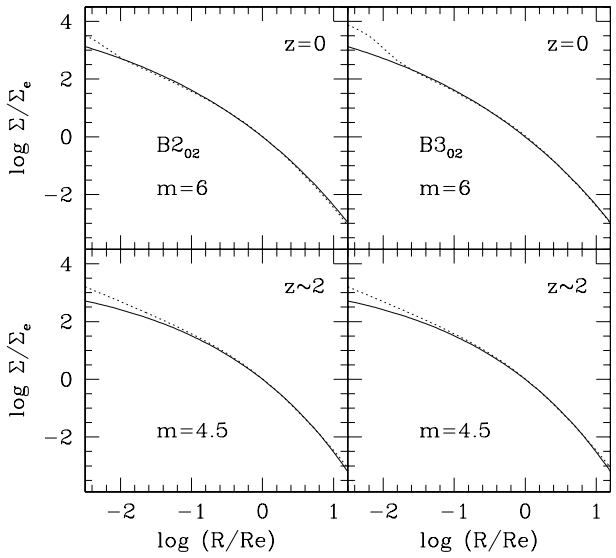

Figure 8. Normalized projected stellar density profiles of models $B2_{02}$ (left panels, dotted lines) and $B3_{02}$ (right panels, dotted lines), near the beginning (bottom panels) and at the end (top panels) of the simulations. Solid lines show the best-fit global Sersic profiles, and the corresponding best-fit index is given. In model $B2_{02}$ the effective radius remains almost unchanged at $R_e = 6.9$ kpc, and the projected mass density is $\Sigma(R_e) \simeq 215\,M_\odot$ pc^{-2}. In model $B3_{02}$ the effective radius contracts from $R_e = 6.9$ kpc to $R_e = 6.2$ kpc, while $\Sigma(R_e)$ increases from $\simeq$215 $M_\odot$ pc^{-2} to $\simeq$263 $M_\odot$ pc^{-2}.

during the burst, mechanical feedback plays a major role in the model evolution, a conclusion that seems to be supported also by observations (Moe et al. 2009; Dunn et al. 2010. We also note that the values deduced for the mechanical feedback efficiency during the burst nicely match the range adopted in the present study, as detailed in Table 1).

We note the general properties of all of the models we have studied. If there is proper allowance for mass conservation, then constraining the models to allow for appropriate SMBH growth *requires* a mechanical efficiency at or below 3×10^{-4}, at least a factor of 10 lower than is commonly assumed. Such a relatively low mechanical efficiency can mean that even outflows driven from as far as 0.1 pc from the SMBH can be important (e.g., Proga et al. 2008; Kurosawa & Proga 2009; Kurosawa et al. 2009).

4.2. The "Best" Models with the Explicit Time-dependent Term in the Nuclear Wind Differential Equation

Before concluding, we briefly illustrate the effects of the inclusion in the simulations of the explicit time-dependent term in the nuclear wind differential equation (Equation (29) in Paper I): we recall that this term takes into account the finite propagation time of the nuclear wind. As can be seen by comparison of Figure 10 with Figure 3, the evolution is somewhat different from the analogous models in which the time-dependent term is suppressed. In general, the temporal structure of the bursts is more complex, a consequence of the additional time-propagation scale of the mechanical feedback, which is out of phase with the global evolution of the galactic gas flows. In fact, as can be seen from Column 13 in Table 1, these B^w models produce a much larger number of bursts than the corresponding B models. However, the total time spent in the high-luminosity state is considerably shorter, as the characteristic burst duration is now (for example) ~1 Myr for models $B2^w_{02}$ and $B3^w_{02}$, rather than ~30 Myr for the models $B2_{02}$ and $B3_{02}$. Overall, the cumulative duty cycle for the new models is reduced by roughly a factor of 10, with $f_{\rm duty} \approx 0.004$.

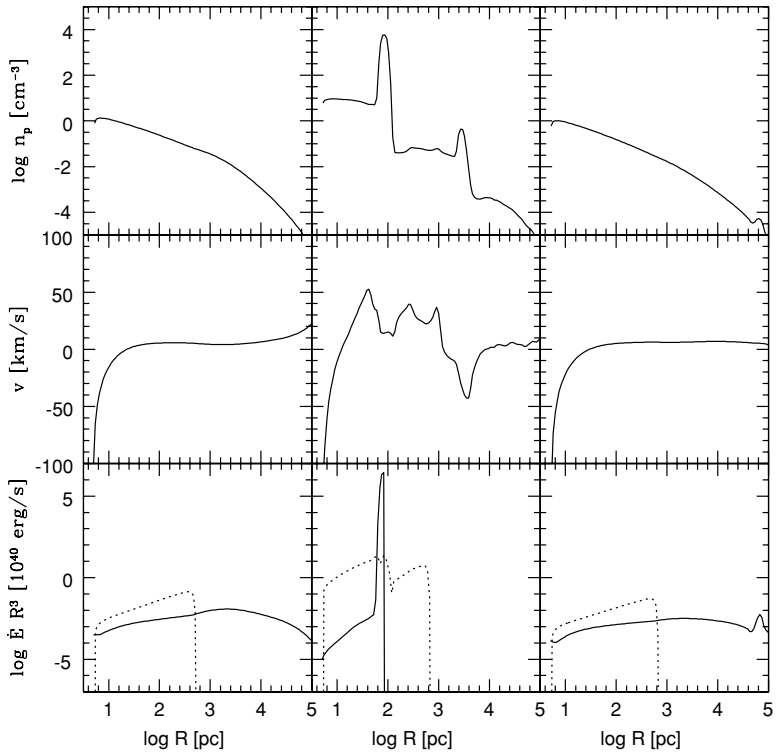

Figure 9. Volume-weighted feedback energy deposition just before (left row), at the end (central row), and after (right row) the first burst of model $B3_{02}$ (bottom panels). Solid lines refer to radiative feedback and solid lines to mechanical feedback. The radial profile of the ISM number density (top panels) and velocity (middle panels) are also shown. Much of the radiation is absorbed in the cold shell at ≈100 pc at the peak of the burst, but at other times the radiative input is broadly distributed. The mechanical energy input from the outflowing wind tends to be more centrally concentrated.

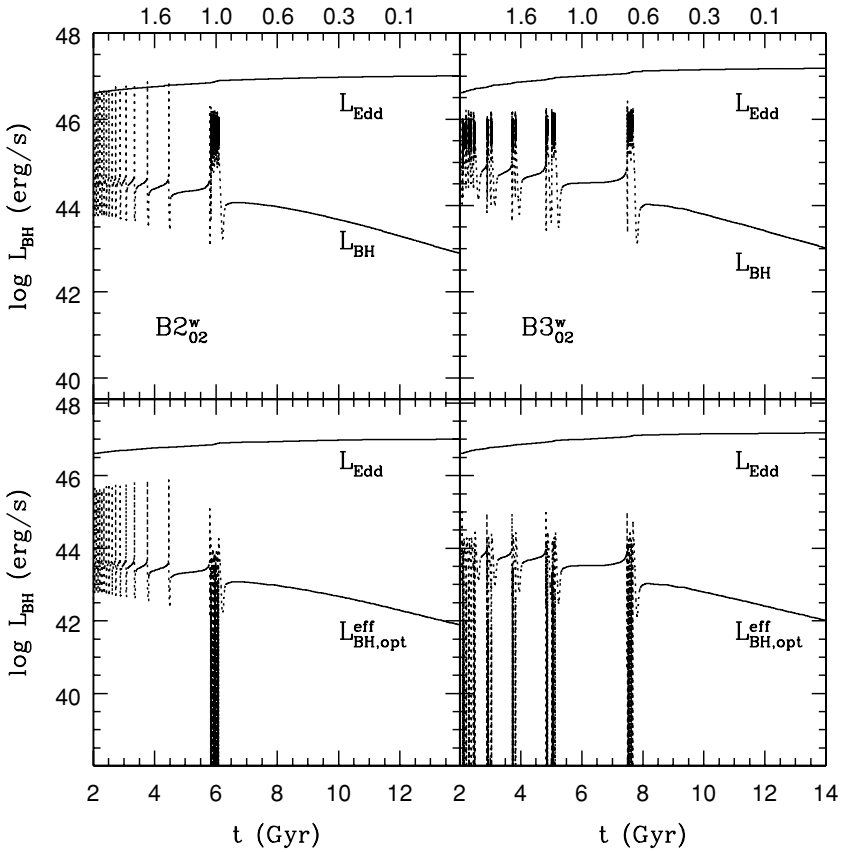

Figure 10. Luminosity evolution of time-dependent wind models $B2^{w}_{02}$ (left panels) and $B3^{w}_{02}$ (right panels). Model quantities are given in Table 1, and lines are as in Figure 3. Comparing these results to those shown in Figure 3 we see qualitatively similar behavior but an even lower duty cycle in the on state, an even more dramatic decline in bursting behavior with decreasing z, and an even lower final luminosity.

From the point of view of the central SMBH, the primary difference is the greater effectiveness of feedback in shutting off accretion, so that the growth of the SMBH is now reduced with respect to B models, and more gas is retained in the galaxy producing an X-ray coronal luminosity 10 times larger. From the point of view of the final stellar distribution, the present models behave similarly to the models described in the previous section, i.e., at the end of the simulation a central "cusp" of new stars is produced, in qualitative agreement with observations. We finally notice how the luminosity-weighted BLR wind solid opening angle (Table 1, Column 12) for this last set of models is found in good agreement with the most recent observational estimates (Lu et al. 2010).

5. DISCUSSION AND CONCLUSIONS

In this paper, we have addressed, with the aid of one-dimensional hydrodynamical simulations, the combined effects of radiative and mechanical feedback from the central SMBH on the gas flows in elliptical galaxies. The investigation is in the line of previous papers, where the input physics and the galaxy models have been substantially improved over time. In Papers I and II, we focused on purely radiative and purely mechanical feedback models, and for both cases we found difficulties in reproducing some of the most important observational features of observed galaxies. In the present paper, we explored the behavior of *combined* models, i.e., when both a physically motivated implementation of radiative and mechanical feedback effects is active in the code.

We briefly recall here the main secure points on which our framework is based. First of all, it is known from stellar evolution theory, and firmly supported by observations, that the recycled gas from dying stars is an important source of fuel for the central SMBH, both in its amount (summing up to 20%–30% of the total mass in stars) and in its availability over cosmic epochs. It is also obvious that the recycled gas, arising from stars in the inner several kpc of the galaxy (assumed a giant elliptical), is necessarily a subject of a classical radiative cooling instability, leading to a collapse toward the center of metal-rich gas. As a consequence, starbursts occur and also the central SMBH is fed. The details of how much is accreted on the central SMBH versus consumed in stars versus ejected from the center by energy input from the starburst and AGN are uncertain. But order of magnitude estimates would have the bulk going into stars or blown out as a galactic wind, with a small amount going into the central SMBH. In addition, since at the end of a major outburst, a hot bubble remains at the center, both processes shut themselves off, and it will take a cooling time for the cycle to repeat. In other words, relaxation oscillations are to be expected, but their detailed character is uncertain. Finally, order of magnitude estimates would indicate that during the bursting phase the center would be optically thick to dust, so one would observe a largely obscured starburst and largely obscured AGN with most radiation in the far-IR; as gas and dust are consumed, the central sources become visible. Much of the AGN output occurs during obscured phases; then there is a brief interval when one sees a "normal" quasar, and finally one would see a low X-ray luminosity and E+A spectrum galaxy,

with A dominating in the central several hundred pc for 10^{7-8} yr. Such figures are consistent with observed statistical occurrence of E+A galaxies in homogeneous samples that are nowadays available (e.g., Goto 2007).

In sum, we find that inclusion of a modest amount of (momentum- and energy-driven mechanical) feedback significantly improves the correspondence with reality, with the optimal level being $\langle\epsilon_{\rm w}\rangle \simeq 10^{-4.5}$. In the models where we took feedback to be 10^2 more efficient, as is commonly assumed, and assuming conservation of both mass and momentum, we found that the results were unsatisfactory with too low an SMBH mass growth and too low thermal X-ray luminosity from the gas. The logic is simple. Very efficient mechanical feedback keeps gas from infalling to the central SMBH and strips the galaxy of thermal gas. In order to better study the problem, we presented three different versions of the same models, namely combined models (type A) in which the mechanical energy associated with the nuclear wind is computed under the assumption of a fixed opening angle for the wind cone; combined models (type B) in which the opening angle of the nuclear wind and the mechanical feedback efficiency are functions of the Eddington normalized instantaneous bolometric luminosity of the SMBH; and finally, in the third family we briefly considered B models with the full differential equation of mechanical feedback, in which the propagation velocity of the nuclear wind is also considered. In each family of models we assumed different (but physically plausible) combinations of parameters.

Overall, we have confirmed the results in CO07, and completed the model investigation in Papers I, II, and V. In more detail, the main results can be summarized as follows.

1. Radiative heating (primarily due to X-rays) without any mechanical energy input greatly reduces the "cooling-flow catastrophe" problem, but leads to a result that is still defective as compared to detailed observations of local elliptical galaxies in that the central SMBH would be too bright and too massive and the galaxy would be too blue at $z = 0$ (CO07, Paper I).
2. Utilizing mechanical energy alone from an AGN wind with fixed efficiency can address the problems but does not give a solution that in detail satisfies the observations (Papers I and II). If the chosen efficiency is large, then we obtain (consistent with Di Matteo et al. 2005 and others) a giant burst and a not too large SMBH, but do not get any late time AGN and the overall duty cycle is too small. If the fixed efficiency is made low enough to avoid these problems, then one simply reverts to case (1) above, the radiative case. Purely mechanical models with luminosity-dependent mechanical efficiency (which seems to be what is indicated both by observations and detailed multi-dimensional hydrodynamical simulations of radiatively driven winds by Proga 2007; Proga et al. 2008; Kurosawa & Proga 2009; Kurosawa et al. 2009) perform better.
3. The combined models explored in this paper, in which both radiative and mechanical feedback are allowed, are clearly better than the two limit cases described above. This family of models, with mechanical energy efficiency proportional to the luminosity, when combined with a realistic treatment of the radiative effects, does seem to be consistent with all observations for a range of efficiencies $\epsilon_{\rm w}$ which includes the values thought to obtain either from an analysis of the observations or from theoretical modeling of the central engines. And, of course, actual observations indicate that both feedback processes do occur: both the radiative output and the broad-line and narrow-line winds are observed from AGNs (e.g., Alexander et al. 2009, 2010).
4. It is found that radiative and mechanical feedback affect different regions of the galaxy at different evolutionary stages. During the "quiescent" phases, when the ISM is optically thin, radiative heating is distributed over all the galaxy body, while the mechanical feedback is deposited in a region of a kpc scale radius. This produces a characteristic feature which is not present in purely radiative models, i.e., the density profile is flatter within $\sim$1 kpc than in models without mechanical feedback. This in turn produces a more flat core in the observed X-ray surface brightness profile (S. Pellegrini et al. 2010, in preparation, Paper IV). However, during the burst, the collapsing cold shells are optically thick, and most of the radiation is intercepted and re-radiated in the IR. It is found that during these short phases it is actually the mechanical feedback that is playing the major role. This means that a proper description of SMBH feedback requires both of the physical components, as discussed in detail in Ostriker et al. (2010).

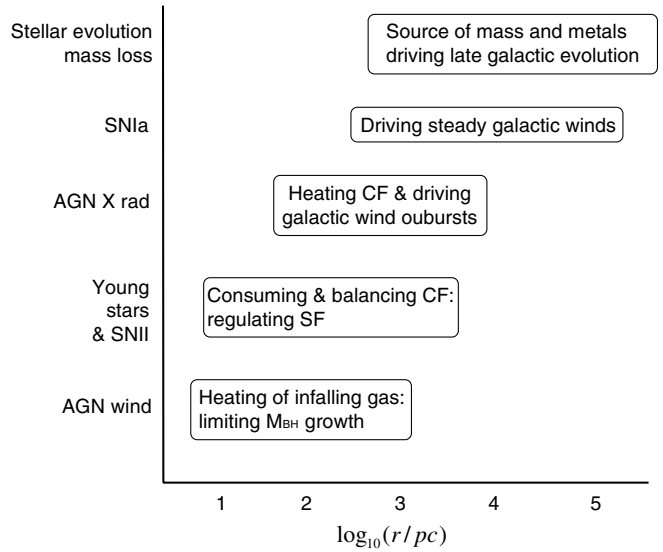

Figure 11. The radial intervals where the different physical mechanisms affect the evolution of gas flows driven by stellar evolution in a representative (isolated) elliptical galaxy.

We summarize the overall situation with a schematic in Figure 11 in which we indicate the spatial regions within which each physical mechanism is dominant. Since the detailed hydro is highly time-dependent, the figure greatly oversimplifies the complex situation but shows the regions where a process is most important during the time interval that it is important.

Tests of the overall picture presented in these papers are numerous and obvious.

1. The E+A spectrum should be found to come from $\lesssim$100 pc regions, be younger, and be significantly more metal rich than the bulk of the stars in a given galaxy.
2. The duration of the AGN bursts should be quite short with regard to cosmic time, say in the range of burst duration $0.3 \lesssim \Delta t \lesssim 30$ Myr.
3. Since satellite galaxies in clusters have more difficulty in retaining the recycled gas than do central galaxies and isolated galaxies, the E+A phenomenon should be rarer

in these systems, the central stellar cusps should be weaker and the incidence of the AGN phenomenon rarer.
4. The fraction of the time that normal elliptical galaxies spend in the bursting state should be small and fairly steeply declining with increasing cosmic time. The final SMBH luminosities will be typically $\sim 10^{-5} L_{\rm Edd}$.
5. If cooling instabilities in recycled gas dominate (at late times) the fueling of AGN bursts, then evidence for merging activity should be relatively rare and the gas seen during the outbursts should be relatively rich in metals (including *S*-process elements).

We conclude by recalling that we restricted our study for simplicity to the case of an isolated elliptical galaxy, therefore excluding the confining or stripping effect of the ICM on the galactic X-ray emitting corona. The two physical phenomena have opposite effects. On one hand, as shown in Shin et al. (2010b), the ram-pressure stripping of the ICM on the galactic atmosphere has the effect of reducing the global X-ray luminosity of the galaxy, and so also to retard or even suppress the cooling catastrophe and the associated AGN bursts. In turn, this will also reduce the starburst activity that we (invariably) find associated with strong bursts. On the other hand, galaxies residing in the central regions of a cluster are presumably more affected by external pressure effects than by ram-pressure stripping. Such galaxies would be on average more X-ray luminous, and show not only larger duty-cycle values, but also younger and bluer nuclear cusps near the SMBH, on the 100 pc scale, than similar galaxies orbiting in the cluster outskirts. Therefore, we expect that the coronal X-ray luminosity of the hot gas, and the number of central bursts of the models presented in this paper, are lower limits for the case of galaxies immersed in a realistic ICM in the central regions of a cluster. Also, the effect of mechanical feedback due to a jet, which is relevant at low accretion luminosities (i.e., during the hot phase accretion common at late times, e.g., see Allen et al. 2006; Merloni & Heinz 2007), is not included. The associated reduction of the accretion luminosity in the low-luminosity states will bring our models nearer to the observed Eddington ratios of low-luminosity AGNs. However, we stress that the maintenance of the SMBH masses to the observed level, in presence of the important amounts of recycled metal-rich gas produced over an Hubble time by the aging stellar populations, is mainly due to the combined effect of the feedback terms included in the simulation, i.e., SNIa and SNII heating, radiative heating, and nuclear wind feedback.

The (metal-rich) recycled gas from stellar evolution is present *even in absence of external phenomena such as galaxy merging or input from cold gas flows*, that are often considered as the natural way to induce quasi-stellar object (QSO) activity. Therefore, one of the main results of our simulations (also considering all the simplifications in the treatment of physics, and of the geometry of the code), is that *the evolution of an isolated galaxy, subject to internal evolution only, can be quite complicated* (e.g., see Pierce et al. 2007), and that AGN feedback will lead to central AGN and starburst activity in many widely spaced brief intervals (e.g., Shi et al. 2009). We note that the possibility of QSO activity, even in the absence of merging, has also been recently proposed also by others (e.g., Li et al. 2008; Kauffmann & Heckman 2009; Tal et al. 2009).

Clearly, the main limitation of the models explored in our series of papers is the adopted spherical symmetry. This choice has been necessary as the main focus of the study has been the understanding of the physics behind AGN feedback. The necessity to explore the parameter space, and the time-expensive numerical integration of heating/cooling, star formation, and radiative transport equations from the pc scale near the SMBH up to the hundred kpc scale of the galaxy outer regions, in the presence of multiple mutually interacting shocks, forced us to use a one-dimensional code. However, we are now working on two-dimensional simulations that allow for a more realistic description of mechanical feedback, of the cold shell stability and fragmentation, and of the effect of angular momentum of the accreting gas. Work performed to date indicates that several aspects of the gas evolution are quite similar in the two-dimensional and one-dimensional simulations.

We thank an anonymous referee for useful comments and suggestions that improved the paper. We also thank Sudeep Das for preparing Figure 1, and Jenny Greene, Tim Heckman, Guinevere Kauffmann, Silvia Pellegrini, and Eliot Quataert for interesting discussions. D.P. acknowledges support by the National Aeronautics and Space Administration under Grant/Cooperative Agreement No. NNX08AE57A issued by the Nevada NASA EPSCoR program. L.C. was supported by the MIUR grant PRIN2008.

REFERENCES

Alexander, D. M., Swinbank, A. M., Smail, I., McDermid, R., & Nesvadba, N. P. H. 2009, in ASP Conf. Ser. 427, Proc. Accretion and Ejection in AGN: A Global View, ed. L. Maraschi et al. (San Francisco, CA: ASP), in press
Alexander, D. M., Swinbank, A. M., Smail, I., McDermid, R., & Nesvadba, N. P. H. 2010, MNRAS, 402, 2211
Allen, S. W., Dunn, R. J. H., Fabian, A. C., Taylor, G. B., & Reynolds, C. S. 2006, MNRAS, 372, 21
Begelman, M. C., & Nath, B. B. 2005, MNRAS, 361, 1387
Begelman, M. C., & Ruszkowski, M. 2005, Phil. Trans. R. Soc. A, 363, 655
Benson, A. J., & Babul, A. 2009, MNRAS, 397, 1302
Binney, J., & Tabor, G. 1995, MNRAS, 276, 663
Brusa, M., et al. 2009, A&A, 507, 1277
Chilingarian, I., De Rijcke, S., & Buyle, P. 2009, ApJ, 697, L111
Ciotti, L. 2009a, La Riv. Nuovo Cimento, 32, 1
Ciotti, L. 2009b, Nature, 460, 333
Ciotti, L., & Bertin, G. 1999, A&A, 352, 447
Ciotti, L., D'Ercole, A., Pellegrini, S., & Renzini, A. 1991, ApJ, 376, 380
Ciotti, L., Morganti, L., & de Zeeuw, P. T. 2009a, MNRAS, 393, 491
Ciotti, L., & Ostriker, J. P. 2001, ApJ, 551, 131
Ciotti, L., & Ostriker, J. P. 2007, ApJ, 665, 1038 (CO07)
Ciotti, L., Ostriker, J. P., & Proga, D. 2009b, ApJ, 699, 89 (Paper I)
Constantin, A., Green, P., Aldcroft, T., Kim, D.-W., Haggard, D., Barkhouse, W., & Anderson, S. 2009, ApJ, 705, 1336
Côté, P., et al. 2006, ApJS, 165, 57
Côté, P., et al. 2007, ApJ, 671, 1456
Davies, R. I., Mueller Sánchez, F., Genzel, R., Tacconi, L., Hicks, E., Friedrich, S., & Sternberg, A. 2007, ApJ, 671, 1388
Davies, R. I., et al. 2009, in IAU Symp. 267, Co-Evolution of Central Black Holes and Galaxies, ed. B. M. Peterson, R. S. Somerville, & T. Storchi-Bergmann (Cambridge: Cambridge Univ. Press), 283
DeBuhr, J., Quataert, E., Ma, C.-P., & Hopkins, P. 2009, arXiv:0909.2872
Diehl, S., & Statler, T. S. 2007, ApJ, 668, 150
Di Matteo, T., Springel, V., & Hernquist, L. 2005, Nature, 433, 604
Dunn, J. P., et al. 2010, ApJ, 709, 611
Goto, T. 2007, MNRAS, 381, 187
Graham, A. W. 2004, ApJ, 613, L33
Graham, A. W., & Driver, S. P. 2005, PASA, 22, 118
Greene, J. E., & Ho, L. C. 2007, ApJ, 670, 92
Haiman, Z., Ciotti, L., & Ostriker, J. P. 2004, ApJ, 606, 763
Heckman, T. M., Kauffmann, G., Brinchmann, J., Charlot, S., Tremonti, C., & White, S. D. M. 2004, ApJ, 613, 109
Ho, L. 2009, ApJ, 699, 626
Hopkins, P. F., Hernquist, L., Cox, T. J., Keres, D., & Wuyts, S. 2009, ApJ, 691, 1424
Jaffe, W. 1983, MNRAS, 202, 995
Jiang, Y.-F., Ciotti, L., Ostriker, J. P., & Spitkovsky, A. 2010, ApJ, 711, 125
Johansson, P. H., Naab, T., & Burkert, A. 2008, Astron. Nachr., 329, 956
Kauffmann, G., & Heckman, T. M. 2009, MNRAS, 397, 135

King, A. 2010, MNRAS, 402, 1516
Kirkman, D., & Tytler, D. 2008, MNRAS, 391, 1457
Kormendy, J., Fisher, D. B., Cornell, M. E., & Bender, R. 2009, ApJS, 182, 216
Kurosawa, R., & Proga, D. 2009, MNRAS, 397, 1791
Kurosawa, R., Proga, D., & Nagamine, K. 2009, ApJ, 707, 823
Lauer, T. R., et al. 2005, AJ, 129, 2138
Lee, J. H., Lee, M. G., Park, C., & Choi, Y.-Y. 2010, MNRAS, 401, 1804
Li, C., Kauffmann, G., Heckman, T. M., White, S. D. M., & Jing, Y. P. 2008, MNRAS, 385, 1903
Lu, Y., Wang, T.-G., Dong, X.-B., & Zhou, H.-Y. 2010, MNRAS, 404, 1761
Magorrian, J., et al. 1998, AJ, 115, 2285
Merloni, A., & Heinz, S. 2007, MNRAS, 381, 589
Moe, M., Arav, N., Bautista, M. A., & Korista, K. T. 2009, ApJ, 706, 525
Naab, T., Johansson, P. H., Ostriker, J. P., & Efstathiou, G. 2007, ApJ, 658, 710
Narayan, R., & Yi, I. 1994, ApJ, 428, L13
Nardini, E., Risaliti, G., Watabe, Y., Salvati, M., & Sani, E. 2010, arXiv:1003.0858
Nayakshin, S., & Power, C. 2010, MNRAS, 402, 789
Nesvadba, N. P. H., Boulanger, F., Salomé, P., Guillard, P., Lehnert, M. D., Ogle, P., Appleton, P., Falgarone, E., & Pineau des Forets, G. 2010, arXiv:1003.3449
Noble, S. C., Krolik, J. H., & Hawley, J. F. 2009, ApJ, 692, 411
Ostriker, J. P., Choi, E., Ciotti, L., Novak, G. S., & Proga, D. 2010, ApJ, submitted (arXiv:1004.2923)
Ostriker, J. P., & Ciotti, L. 2005, Phil. Trans. R. Soc. A, 363, 667
Pellegrini, S. 2005, ApJ, 624, 155
Pellegrini, S., & Ciotti, L. 1998, A&A, 333, 433
Pellegrini, S., Ciotti, L., & Ostriker, J. P. 2009, Adv. Space Res., 44, 340
Pierce, C. M., et al. 2007, ApJ, 660, L19
Proga, D. 2007, in ASP Conf. Ser. 373, The Central Engine of Active Galactic Nuclei, ed. L. C. Ho & J.-M. Wang (San Francisco, CA: ASP), 267
Proga, D., & Kallman, T. 2004, ApJ, 616, 688
Proga, D., Ostriker, J. P., & Kurosawa, R. 2008, ApJ, 676, 101
Proga, D., Stone, J. M., & Kallman, T. 2000, ApJ, 543, 686
Rafanelli, P., Vaona, L., D'Abrusco, R., Ciroi, S., & Cracco, V. 2010, in Proc. 1st International Workshop, Astrophysical Winds and Disks (Trieste: Memorie della Società Astronomica Italiana), in press (arXiv:1001.0337v2)
Renzini, A. 2006, ARA&A, 44, 141
Renzini, A., Ciotti, L., D'Ercole, A., & Pellegrini, S. 1993, ApJ, 419, 52
Rodighiero, G., et al. 2007, MNRAS, 376, 416
Salim, S., & Rich, R. M. 2010, ApJ, 714, L290
Sazonov, S. Yu., Krivonos, R., Revnivtsev, M., Churazov, E., & Sunyaev, R. A. 2008, A&A, 482, 517
Sazonov, S. Yu., Ostriker, J. P., Ciotti, L., & Sunyaev, R. A. 2005, MNRAS, 358, 168
Sazonov, S. Yu., Ostriker, J. P., & Sunyaev, R. 2004, MNRAS, 347, 144
Sazonov, S. Yu., Revnivtsev, M., Krivonos, R., Churazov, E., & Sunyaev, R. A. 2007, A&A, 462, 57
Schawinski, K., et al. 2009, ApJ, 690, 1672
Schlesinger, K., Pogge, R. W., Martini, P., Shields, J. C., & Fields, D. 2009, ApJ, 699, 857
Sersic, J. L. 1968, Atlas de Galaxias Australes (Cordoba: Observatorio Astronomico)
Shapiro, K. L., et al. 2010, MNRAS, 402, 2140
Shi, Y., Rieke, G. H., Ogle, P., Jiang, L., & Diamond-Stanic, A. M. 2009, ApJ, 703, 1107
Shin, M. S., Ostriker, J. P., & Ciotti, L. 2010a, ApJ, 711, 268 (Paper II)
Shin, M. S., Ostriker, J. P., & Ciotti, L. 2010b, ApJ, submitted (arXiv:1003.1108)
Sijacki, D., Pfrommer, C., Springel, V., & Ensslin, T. A. 2008, MNRAS, 387, 1403
Springel, V., Di Matteo, T., & Hernquist, L. 2005, MNRAS, 361, 776
Tal, T., van Dokkum, P. G., Nelan, J., & Bezanson, R. 2009, AJ, 138, 1417
Tang, Y., Gu, Q.-S., Huang, J.-S., & Wang, Y.-P. 2009, MNRAS, 397, 1966
Thompson, T. A., Quataert, E., & Murray, N. 2005, ApJ, 630, 167
Wang, T., Zhou, H., Yuan, W., Lu, H. L., Dong, X., & Shan, H. 2009, ApJ, 702, 851
Wild, V., Heckman, T., & Charlot, S. 2010, MNRAS, in press (arXiv:1002.3156)
Yu, Q., & Tremaine, S. 2002, MNRAS, 335, 965